ACS NANO

www.acsnano.org

REVIEW

Heteroatom Immobilization Engineering toward High-Performance Metal Anodes

Jianan Gu, Yongzheng Zhang,* Yu Shi, Yilong Jin, Hao Chen, Xin Sun, Yanhong Wang, Liang Zhan, Zhiguo Du,* Shubin Yang,* and Meicheng Li*

Cite This: *ACS Nano* 2024, 18, 25966–25985

Read Online

ACCESS | Metrics & More | Article Recommendations

ABSTRACT: **Heteroatom immobilization engineering (HAIE) is becoming a forefront approach in materials science and engineering, focusing on the precise control and manipulation of atomic-level interactions within heterogeneous systems. HAIE has emerged as an efficient strategy to fabricate single-atom sites for enhancing the performance of metal-based batteries. Despite the significant progress achieved through HAIE in metal anodes for metal-based batteries, several critical challenges such as metal dendrites, side reactions, and sluggish reaction kinetics are still present. In this review, we delve into the fundamental principles underlying heteroatom immobilization engineering in metal anodes, aiming to elucidate its role in enhancing the electrochemical performance in batteries. We systematically investigate how HAIE facilitates uniform nucleation of metal in anodes, how HAIE inhibits side reactions at the metal anode−electrolyte interface, and the role of HAIE in promoting the desolvation of metal ions and accelerating reaction kinetics within metal-based batteries. Finally, we discuss various strategies for implementing HAIE in electrode materials, such as high-temperature pyrolysis, vacancy reduction, and molten-salt etching and anchoring. These strategies include selecting appropriate heteroatoms, optimizing immobilization methods, and constructing material architectures. They can be utilized to further refine the performance to enhance the capabilities of HAIE and facilitate its widespread application in next-generation metal-based battery technologies.**

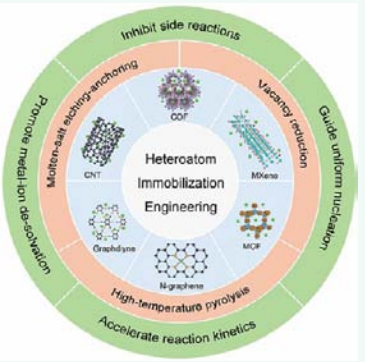

KEYWORDS: *heteroatom immobilization engineering, single-atom sites, nucleation and growth, metal anodes, metal dendrite, desolvation kinetics, hydrogen evolution reaction, side reactions, and zinc-ion battery*

1. INTRODUCTION

Heteroatom immobilization engineering (HAIE) is becoming a forefront approach in materials science and engineering, focusing on the precise control and manipulation of atomic-level interactions within heterogeneous systems.[1−6] Through strategic placement or bonding of foreign atoms within host materials, HAIE enables the synthesis of a diverse array of materials, including single-atom materials, binary atomic materials, single-atom nanoisland, single-atom arrays, and single-atom alloys.[7−23] HAIE provides opportunities to regulate the physical and chemical properties of nanomaterials, leading to enhanced performance in various applications. This innovative technique has garnered significant attentions across multiple disciplines due to its versatility and potential to address the pressing issues in energy storage, catalysis, sensor, and beyond.[24−27]

In the field of energy storage, HAIE has emerged as a promising strategy to fabricate single-atom sites for enhancing the performance of metal-based batteries.[4,9,28] These batteries, composed of metallic anodes such as Li, Na, or Zn, and cathodes such as S or Se, have gained widespread interest as efficient and scalable energy storage devices for broad applications.[29−33] However, some inherent limitations such as low energy density, short cycling stability, and safety concerns, including those associated with metal dendrite formation on anodes, detrimental side reactions, and sluggish reaction kinetics, have spurred intensive research efforts to overcome these challenges.[34−41] HAIE holds great potential to address the above issues by precisely tailoring the atomic structure and surface properties of electrode materials in various batteries. This is primarily achieved through the utilization of single atoms, featured with low atomic content, but maximum atom utilization and high activity.[42−47] By implanting heteroatoms such as Zn, Cu, Co within or on the

Received: July 2, 2024
Revised: August 29, 2024
Accepted: September 5, 2024
Published: September 11, 2024

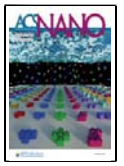

lattice of electrode materials, such as MXenes, MOFs, N-graphene, graphdiyne, CNT, and COFs, HAIE facilitates the optimization of electrochemical performance by inducing flat anode surface, suppressing side reactions, enhancing metal ion transfer kinetics, and improving structural stability.[27,48−54] For instance, carbon-based materials such as N-graphene, graphdiyne, and CNT are commonly used as substrates for loading single atoms due to their ability to easily bond thick metal-N_x configurations. MOFs and COFs, with their naturally uniform single-atom metal structures, often provide high-loading single-atom sites through pyrolysis methods. In addition, MXenes can also anchor single atoms using their abundant vacancies and surface functional groups. Moreover, HAIE enables the design of electrode materials with customized interfaces and synergistic effects, thereby resulting in superior electrochemical properties and an extended battery lifespan (Figure 1).[28,55−58]

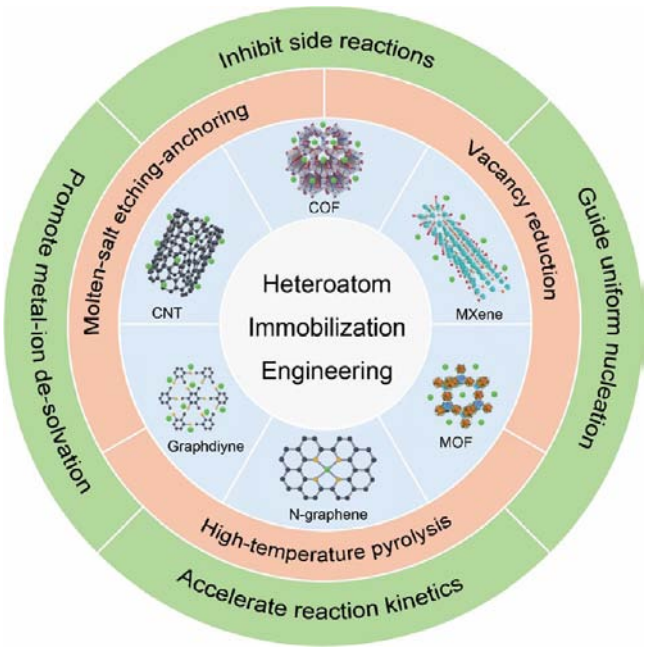

Figure 1. Schematic illustration of heteroatom immobilization engineering applied in metal anodes.

Despite of the significant progress achieved through HAIE in metal-based batteries, several critical challenges are still present.[59,60] First of all, whether single-atom sites continue to play a role in the subsequent stage of metal growth remains to be studied. Although the initial nucleation of crystals determines the subsequent growth state, the metal growth often leads to structural deformations or defects, introducing uncertainties in a later stage. Single-atom sites could inhibit hydrogen evolution and obstruct the polysulfide shuttle effect but may also introduce undesirable side reactions such as the OER or organic electrolyte decomposition. Therefore, balancing the benefits and drawbacks of different reactions when selecting single-atom materials is crucial. Additionally, the effectiveness of single-atom sites in various solvation environments needs further investigation, especially under low-temperature conditions where metal-ion desolvation and reaction kinetics are slower. Furthermore, the development of scalable synthesis methods for producing heterogeneous atom-immobilized electrode materials, understanding the underlying mechanisms governing the electrochemical behavior, and addressing potential issues related to long-term stability and commercial viability are essential.[61−63] Thus, continuous efforts are still needed to overcome these hurdles and unlock the potential of HAIE for advanced metal-based batteries.

Herein, we first delve into the fundamental principles underlying heteroatom immobilization engineering in metal-based batteries, aiming to elucidate its role in enhancing the performance of batteries. Through strategically immobilizing heteroatoms, HAIE aims to tailor the atomic structure and surface properties of the anode material, thereby optimizing its electrochemical performance. Then, we investigate how HAIE facilitates uniform nucleation of metal in anodes. Through the controllable placement or bonding of foreign atoms, HAIE promotes homogeneous nucleation of metal ions during charge and discharge processes. Furthermore, we investigate how HAIE functions to inhibit side reactions at the anode−electrolyte interface. Through incorporating selected heteroatoms into the electrode materials or artificial solid-electrolyte interphase (SEI) film, HAIE minimizes harmful chemical reactions that can degrade the performance of batteries over time. Additionally, we explore the role of HAIE in promoting the desolvation of metal ions and accelerating reaction kinetics within the metal-based batteries. Through the precise immobilization of heteroatoms, HAIE could modify the solvation environment around metal ions, facilitating their rapid desolvation and subsequent intercalation into the electrode material during battery operation. Finally, we discuss various strategies for implementing HAIE in electrode materials, including the selection of appropriate heteroatoms, optimization of the immobilization methods, and construction of material architectures. By refining battery performance, these strategies not only amplify HAIE's capabilities but also facilitate its broad adoption in next-generation metal-based battery technologies.

2. WORKING PRINCIPLE OF HETEROATOM IMMOBILIZATION ENGINEERING IN METAL ANODES

Metal anodes are critical components in energy storage batteries, serving as the primary sites for electrochemical reactions during charge−discharge cycles. The electrochemical performance of anodes significantly influences the overall efficiency, energy density, and cycling stability of battery systems.[64−66] However, metal anodes are confronted with various challenges that hinder their widespread application in practical battery devices. One of the prominent issues is the uncontrollable formation of metal dendrites in anodes during cycling, which can compromise battery performance and cause serious safety issues.[67−69] Dendrites have branching structures that form on the surface of anodes because of nonuniform nucleation and uneven metal-ion flux during repeated charge and discharge processes. These dendrites can lead to internal short circuits, reduced cycling stability, and even safety hazards, as well as battery failure. Besides, the growth of metal dendrites can exacerbate the consumption of the electrolyte in both organic and aqueous environments, leading to further sluggishness in reaction kinetics.[70−74]

To address the challenges related to metal anodes, various strategies have been proposed, including the development of controllable nucleation, stress-release, protective coatings, electrolyte additives, and advanced electrode architectures.[75−78] Among these strategies, HAIE has emerged as a

https://doi.org/10.1021/acsnano.4c08831
ACS Nano 2024, 18, 25966−25985

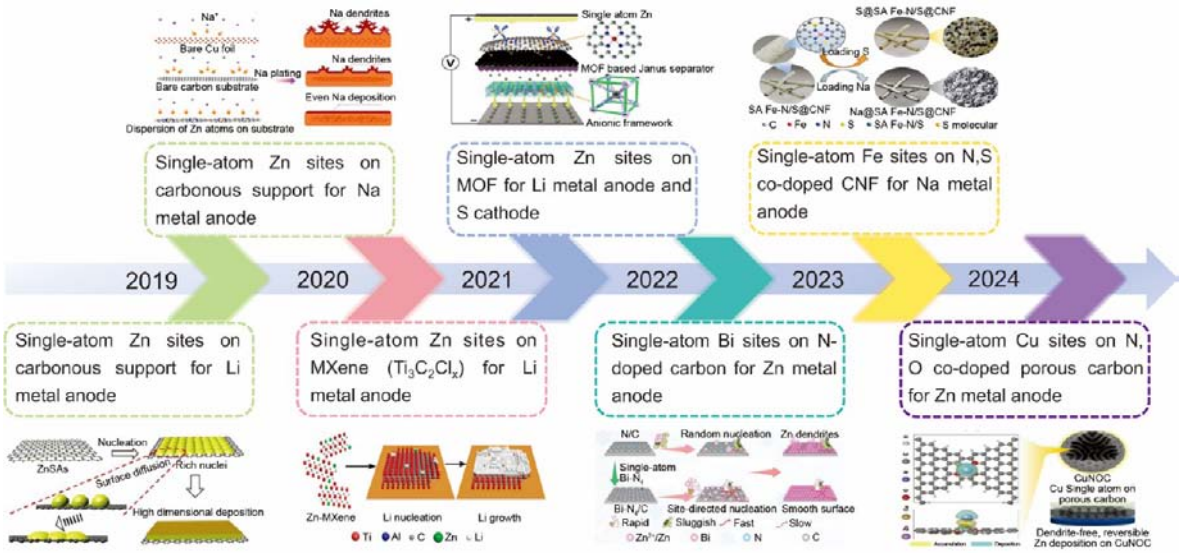

Figure 2. Timeline of heteroatom immobilization engineering on metal anodes. Single-atom Zn sites on carbonous support for Li metal anode. Reproduced with permission from ref 79. Copyright 2019 Elsevier. Single-atom Zn sites on carbonous support for Na metal anode. Reproduced with permission from ref 80. Copyright 2019 American Chemical Society. Single-atom Zn sites on MXene ($Ti_3C_2Cl_x$) for Li metal anode. Reproduced with permission from ref 81. Copyright 2020 American Chemical Society. Single-atom Zn sites on MOF for Li metal anode and S cathode. Reproduced with permission from ref 82. Copyright 2021 American Chemical Society. Single-atom Bi sites on N-doped carbon for Zn metal anode. Reproduced with permission from ref 83. Copyright 2022 American Chemical Society. Single-atom Fe sites on N,S-codoped CNF for Na metal anode. Reproduced with permission from ref 84. Copyright 2023 Wiley-VCH. Single-atom Cu sites on N,O-codoped porous carbon for Zn metal anode. Reproduced with permission from ref 45. Copyright 2024 Wiley-VCH.

Figure 3. Working principle of heteroatom immobilization engineering in metal anodes.

promising approach to induce uniform nucleation in metal anodes and mitigate dendrite formation. For instance, by harnessing the lithiophilic feature, Qian et al. adopted single-atom Zn sites on carbon-based materials to guide uniform Li plating in 2019.[79] In the same year, Yan and his co-workers applied single-atom Zn sites to guide Na nucleation.[80] Subsequently, in 2020, our group introduced Zn atoms onto MXene layers to induce homogeneous Li deposition.[81] Afterward, Lan et al. introduced Zn atoms on an MOF-based separator, achieving stable Li-S batteries.[82] In the following years, other single-atom systems, such as Bi,[83] Fe,[84] and Cu,[85] were developed, giving rise to a uniform surface of metal anodes in Na-S and aqueous Zn-ion batteries (Figure 2).

In the case of the working principle of HAIE in metal anodes, it is essential to delve into the intricate details of how this process operates at the atomic level. HAIE involves the precise immobilization of heteroatoms within/on the lattice of metal anodes, aiming to tailor their atomic structure and surface properties. By strategically positioning heteroatoms such as Zn, Cu, Co, HAIE promotes uniform nucleation of metal ions during charge/discharge cycles, thereby suppressing dendrite formation and prolonging the cycle life of anodes.[76,86,87] The introduction of heteroatoms into the metal lattice creates localized variations in electron density and potential energy landscapes, serving as preferential sites for the adsorption and nucleation of metal ions and leading to uniform deposition of metal ions during electrochemical cycling. Additionally, HAIE can mitigate side reactions that may occur at the surface of anodes, leading to improved cycling stability and prolonged battery lifespan.[45,88] For instance, Cu atoms have a stronger adsorption effect on free hydrogen, which could increase the activation energy for the production of hydrogen gas in aqueous environments, thereby inhibiting the hydrogen evolution reaction. Similar functions could also be achieved with single-atom materials with Sn, Ga, and In. Besides, one of the key aspects of HAIE is its ability to influence the energy barriers associated with ion migration and electron transfer occurring at the anode−electrolyte interface.[37,89] By altering these energy barriers, HAIE can enhance the kinetics of electrochemical reactions, facilitating fast ion transport and charge transfer. This enhancement is particularly important for high-rate applications, where sluggish reaction kinetics can limit battery performance (Figure 3).

HAIE represents a sophisticated approach to engineer the atomic structure and surface properties of metal anodes with the aim of optimizing their electrochemical performance. HAIE enhances metal anode performance in batteries by strategically placing heteroatoms such as Zn, Cu, and Co within or on the anode lattice. This precise immobilization promotes uniform nucleation of metal ions, suppressing

https://doi.org/10.1021/acsnano.4c08831
ACS Nano 2024, 18, 25966−25985

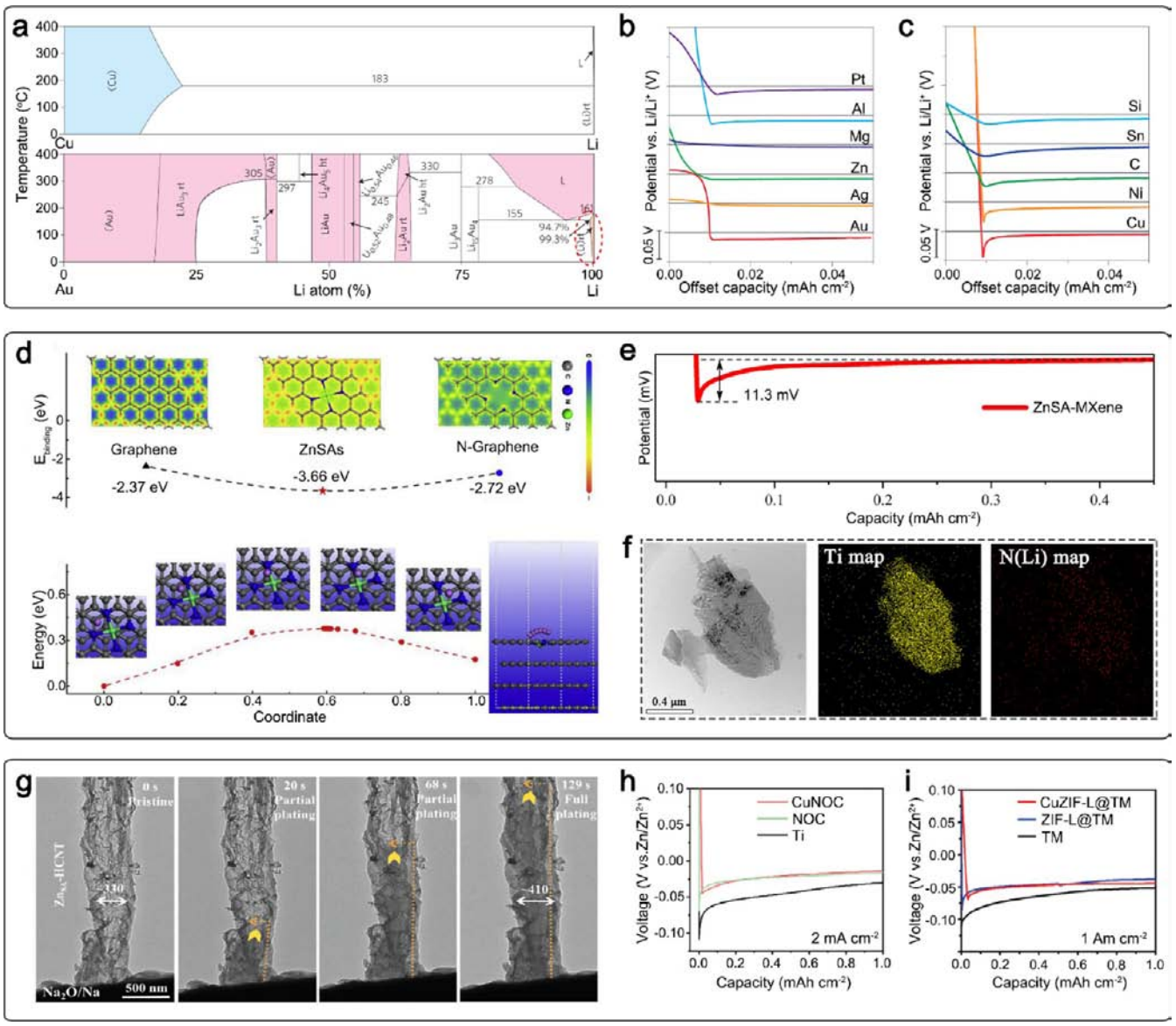

Figure 4. (a) Phase diagrams of Li with Cu (up) and Au (bottom). The region where Au dissolved in Li is circled by the dashed line. L refers to liquid and (Li)rt means lithium metal phase at room temperature. (b) Voltage profiles of various materials with some solubility in Li during Li deposition at a current density of 10 μA cm^{-2}. (c) Voltage profiles of various materials with negligible solubility in Li during Li deposition at 10 μA cm^{-2}. The horizontal gray lines show 0 V versus Li in (b) and (c).[93] Reproduced with permission from ref 93. Copyright 2016 Nature Publishing Group. (d) Electron density difference and surface binding energy of graphene, ZnSAs, and N-graphene, and Li migration pathways and barriers on ZnSAs.[79] Reproduced with permission from ref 93. Copyright 2019 Elsevier. (e) Voltage−capacity curves of lithium plating on the resultant ZnSA-MXene measured at 50 μA cm^{-2}, showing a low overpotential of 11.3 mV. (f) STEM and elemental mapping images of ZnSA-MXene-Li layers at the plating level of 0.1 μAh cm^{-2} after nitriding treatment.[81] Reproduced with permission from ref 81. Copyright 2019 American Chemical Society. (g) *In situ* TEM observation of a typical Na plating process on a ZnSA-HCNT.[90] Reproducedwith permission from ref 90. Copyright 2022 Wiley-VCH. (h) Nucleation overpotential profiles of CuNOC, NOC, and Ti electrodes at 2 mA cm^{-2}.[85] Reproduced with permission from ref 85. Copyright 2024 Wiley-VCH. (i) Voltage profiles of Zn plating on CuZIF-L@TM, ZIF-L@TM, and TM hosts at 1 mA cm^{-2}.[94] Reproduced with permission from ref 94. Copyright 2022 Wiley-VCH.

dendrite formation, which improves cycling stability and prevents safety issues. HAIE also mitigates side reactions on the anode surface, prolonging the battery lifespan. Furthermore, HAIE modifies the local chemical environment, enhancing ion transport rates and charge transfer efficiency, thereby optimizing the electrochemical processes at the anode−electrolyte interface. Through precise manipulation of atomic interactions, HAIE offers a promising pathway toward the development of high-performance metal-based batteries for various energy storage applications.

3. HETEROATOM IMMOBILIZATION ENGINEERING TO INDUCE UNIFORM NUCLEATION IN METAL ANODES

Dendrite formation and uneven deposition during charge and discharge cycles have impeded the widespread adoption of metal anodes. In response to these challenges, researchers have sought many innovative solutions among which heteroatom immobilization engineering stands out. In this section, we investigate the applications of HAIE for fabricating single-atom sites to induce uniform nucleation in metal anodes, under-

https://doi.org/10.1021/acsnano.4c08831
ACS Nano 2024, 18, 25966−25985

Table 1. Electrochemical Performance of Various Metal-Based Anodes with Single-Atom Sites for Energy Storage

Anode types	Single-atom	Hosts	Nucleation overpotential	Anode performance	Full cell performance	Ref.
Li	Zn	N-graphene	~12 mV at 0.5 mA cm^{-2}	800 h at 1 mA cm^{-2}, 1 mAh cm^{-2}	100 cycles for Li-O_2 at 0.1 A g^{-1}	79
Li	Zn	MXene	~11 mV at 0.05 mA cm^{-2}	1200 h at 1 mA cm^{-2}, 1 mAh cm^{-2}	500 cycles with LFP at 10 C	81
Na	Zn	Hollow CNT	~7.4 mV at 5 mA cm^{-2}	900 h at 10 mA cm^{-2}, 1 mAh cm^{-2}	200 cycles with PB at 0.2 C	90
Na	Zn	N-carbon	~0 mV at 0.5 mA cm^{-2}	1000 h at 0.5 mA cm^{-2}, 0.5 mAh cm^{-2}	1000 cycles with NVP at 0.5 C	80
Zn	Cu	N, O-carbon	~28 mV at 2 mA cm^{-2}	~800 h at 5 mA cm^{-2}, 5 mAh cm^{-2}	400 cycles with V_2O_5 at 0.5 A g^{-1}	85
Zn	Cu	ZIF	~25 mV at 1 mA cm^{-2}	1100 h at 1 mA cm^{-2}, 1 mAh cm^{-2}	1000 cycles with V_2O_5 at 1 A g^{-1}	94
Zn	Bi	N-carbon	~39 mV at 0.5 mA cm^{-2}	840 h at 5 mA cm^{-2}, 1 mAh cm^{-2}	1000 cycles with KVOH at 1 A g^{-1}	83
Li	Co	N-graphene	~16 mV at 1 mA cm^{-2}	800 h at 2 mA cm^{-2}, 2 mAh cm^{-2}	~350 cycles with LFP at 1 C	91
Li	Co	N-Carbon	~12.3 mV at 1 mA cm^{-2}	2000 h at 1 mA cm^{-2}, 1 mAh cm^{-2}	~300 cycles with LFP at 0.2 C	92
K	Co	N-Carbon	~3 mV at 0.5 mA cm^{-2}	2400 h at 0.5 mA cm^{-2}, 0.5 mAh cm^{-2}	200 cycles with PTCDA at 0.2 A g^{-1}	95
NaK	Co	Carbon	/	4000 h at 10 mA cm^{-2}, 10 mAh cm^{-2}	20000 cycles with NVP at 10 C	96
Li	Co	Graphene	10.5 mV at 1 mA cm^{-2}	800 h at 1 mA cm^{-2}, 1 mAh cm^{-2}	1000 cycles with S at 0.5 C	97
Li	Co	N,O-Carbon	28.8 mV at 1 mA cm^{-2}	2000 h at 1 mA cm^{-2}, 1 mAh cm^{-2}	/	87
Li	Mn	N-graphene	~10 mV at 0.5 mA cm^{-2}	600 h at 1 mA cm^{-2}, 1 mAh cm^{-2}	210 cycles with LFP at 1 C	86
Zn	Zn	N-carbon	15 mV at 1 mA cm^{-2}	750 h at 1 mA cm^{-2}, 1 mAh cm^{-2}	1000 cycles with S-PANI at 5 A g^{-1}	88
Zn	Co	N-carbon	38.5 mV at 1 mA cm^{-2}	2000 h at 1 mA cm^{-2}, 1 mAh cm^{-2}	8000 cycles with V_2O_5 at 1 A g^{-1}	101
Li	Co	MOF	53 mV at 2 mA cm^{-2}	400 h at 2 mA cm^{-2}, 1 mAh cm^{-2}	600 cycles with S at 1 C	102
Li	Co	N-carbon	10 mV at 1 mA cm^{-2}	1500 h at 3 mA cm^{-2}, 3 mAh cm^{-2}	600 cycles with S at 0.2 C	103
Li	Co	Porous carbon	/	1500 h at 0.5 mA cm^{-2}, 0.5 mA cm^{-2}	100 cycles with S at 0.5 C	104
Li	Co/Fe	ZIF-8	/	/	500 cycles with S at 1 C	105
Li	Zn	Carbon sphere	15 mV at 1 mA cm^{-2}	1200 h at 3 mA cm^{-2}, 3 mAh cm^{-2}	700 cycles with S at 5 C	106
Li	Zn	MOF-100	/	2800 h at 5 mA cm^{-2}, 10 mAh cm^{-2}	1000 cycles with S at 2 C	82
Li	Mo	N-graphene	/	1000 h at 0.5 mA cm^{-2}, 0.5 mA cm^{-2}	500 cycles with S at 1 C	107
Li	Ru	rGO	/	400 h at 1 mA cm^{-2}, 1 mAh cm^{-2}	800 cycles with S at 1 C	108
Na	Fe	N-carbon	13.7 mV at 1 mA cm^{-2}	500 h at 1 mA cm^{-2}, 1 mAh cm^{-2}	500 cycles with S at 1 C	84
Na	Y	MOF	22.4 mA at 1 mA cm^{-2}	1700 h at 3 mA cm^{-2}, 3 mAh cm^{-2}	1000 cycles with S at 5 A g^{-1}	109
Li	Co	COF	8 mA at 0.5 mA cm^{-2}	4000 h at 5 mA cm^{-2}, 5 mAh cm^{-2}	650 cycles with LFP at 1 C	89

scoring its significance in metal-based batteries. HAIE can introduce metallophilic (lithiophilic/sodiophilic/zincophilic) sites to guide metal nucleation, which can be categorized into two types: 1) the heteroatoms with electrochemical activity can react with the deposited metals to form alloys at the metal anode, serving as nucleation sites for metal deposition;[76,90] 2) the heteroatoms with a specific coordination environment and electronic structure to the substrate materials through bonding such as Co-N_x could be employed as active sites for the nucleation of metals.[91,92]

3.1. Metallophilic Sites with Electrochemical Activity.

Cui and his co-workers put forward the "heterogeneous seeded growth" strategy, which is based on the solubility of heterogeneous metals within lithium in metallic Li anodes.[93] They discovered that there is no nucleation barrier when heterogeneous metals exhibit infinite solubility in Li (Figure 4a). Moreover, it is demonstrated that many heterogeneous metals, such as Au, Ag, Zn, and Mg, are favorable for Li nucleation by significantly reducing the nucleation barriers (Figure 4b and 4c). Based on this, Qian et al. fabricated a lithiophilic Zn atoms on N-graphene nanomaterial (Zn-N-graphene coordination) as a substrate to bear the Li deposition.[79] Benefiting from the abundant lithiophilic sites enabled by single-atom Zn, the deposited Li has a flat surface without dendrites. Theoretical calculations reveal that the Zn-N-graphene configuration has a higher surface binding energy as well as lower migration barriers with Li atoms (Figure 4d), highly enhancing the Li transfer kinetics. Besides, the improved transfer kinetics on Zn-N-graphene results in a low overpotential (~12 mV) and a high Coulombic efficiency (CE, ~99.99%). The symmetrical Li-Zn-N-graphene cells exhibit stable cycling performance for more than 800 h with smooth voltage oscillations (Table 1). As a result, these findings contribute to a deeper comprehension of the electrochemical deposition mechanisms for Li anodes and illustrate the function of single Zn atoms to benefit Li nucleation. Furthermore, to explore the behavior of single Zn atoms in guiding Li nucleation, our research group utilized MXene nanomaterials to anchor Zn atoms (ZnSA-MXene) as the substrate for Li plating.[81] We initially collected the Li nucleation curves and observed a low overpotential of ~11 mV (Figure 4e), which is comparable to that of Zn-N-graphene (~12 mV). This indicates that the single-atom Zn can serve as a nucleating agent to benefit lithium deposition as it is incorporated into different host materials. Consequently, when ZnSA-MXene-Li is utilized as a lithium anode, a long cycling life of 1200 h as well as a high stripping-plating levels of up to 40 mAh cm^{-2} are obtained (Table 1). Furthermore, *ex situ* TEM measurement has revealed that Li element is homogeneously dispersed on the surface of MXene layers in the initial plating stage (Figure 4f).[81] This observation demonstrates that the ZnSA-MXene layers facilitate uniform nucleation of Li because of the existence of abundant lithiophilic Zn sites. This study provides the possibility of utilizing single-atom MXenes for promoting homogeneous metal nucleation in other metal-anode systems. However, it is worth noting that this study lacks real-time observation of metal nucleation on lithiophilic Zn atoms by TEM.

To address this issue, Dong et al. turned their focus to Na deposition on Zn atoms.[90] This choice was made because Na could withstand TEM electron radiation and shares similar properties to Li. They employed a hollow carbon nanotube

https://doi.org/10.1021/acsnano.4c08831
ACS Nano 2024, 18, 25966−25985

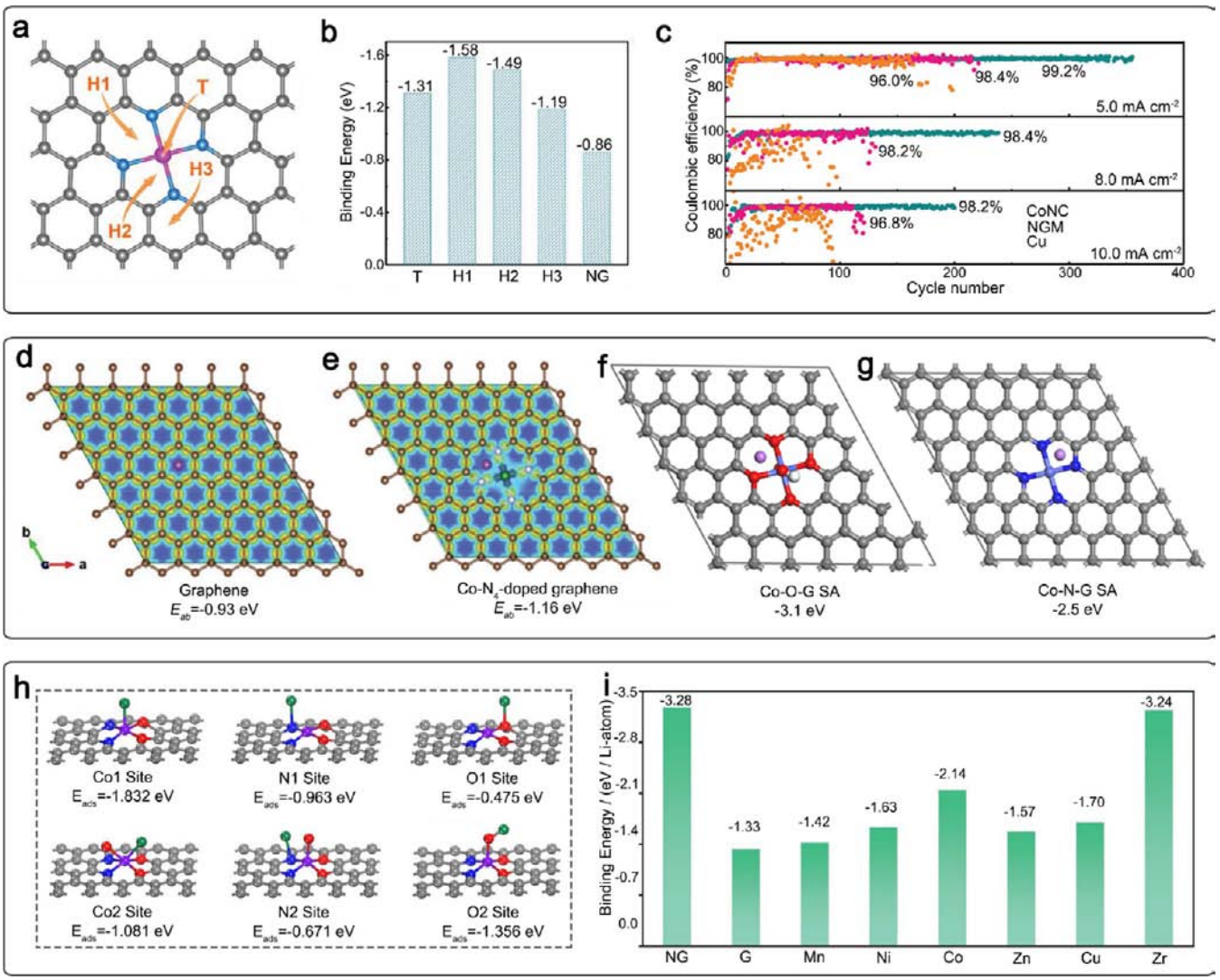

Figure 5. (a) Li adsorption sites on CoNC. The carbon, nitrogen, and cobalt are marked with gray, blue, and deep pink balls, respectively. (b) The summary of binding energies between a Li atom and different adsorption sites on CoNC. (c) CE of CoNC, NGM, and Cu electrodes at a fixed capacity of 2.0 mAh cm^{-2}.[91] Reproduced with permission from ref 91. Copyright 2018 Wiley-VCH. (d) Optimized structures and deformation charge density of K atom adsorption site on ideal (d) graphene sheet and (e) Co-N_4-doped graphene.[95] Reproduced with permission from ref 95. Copyright 2023 Wiley-VCH. Binding energy of a Li atom with (f) Co-O-G SA and (g) Co-N-G SA, where C, O, N, H, and Li atoms are represented by gray, red, blue, white, and purple balls, respectively.[97] Reproduced with permission from ref 97. Copyright 2021, by Chinese Chemical Society. (h) Adsorption structures and corresponding adsorption energies of Co-N/O-500 toward Li^+.[87] Reproduced with permission from ref 87. Copyright 2022 Wiley-VCH. (i) Binding energy of Li atoms on different substrates including graphene, NG, SAMn@NG, SANi@NG, SACo@NG, SAZn@NG, SACo@NG, and SAZr@NG.[86] Reproduced with permission from ref 86. Copyright 2022 Wiley-VCH.

with Zn atoms incorporated into the carbon shell (ZnSA-HCNT) for investigating the Na nucleation behaviors. Through *in situ* TEM measurements, the nucleation process of Na metal on ZnSA-HCNT can be directly observed. The Na metal gradually grows into the interspace of the carbon nanotube due to the sodiophilic Zn atoms filled interiorly (Figure 4g). This provides direct evidence that single atom Zn sites possess the function of Na nucleation. Consequently, the Na@ZnSA-HCNT anode exhibits a good long-term property in symmetrical batteries (>900 h at 10 mA cm^{-2}) and demonstrates an excellent electrochemical performance in full cells (Table 1).[90] Similarly, Yan et al. proposed a nanocomposite consisting of a nitrogen-doped carbon substrate and Zn single atoms (ZnSA-N-carbon) as a current collector for metallic Na deposition.[80] Interestingly, a nucleation overpotential close to zero was achieved in ZnSA-based anodes associated with a good nucleation behavior, significantly lower than the previously reported substrates. As a result, the ZnSA-N-carbon-Na anode exhibits a high Na stripping/plating CE of over 99.8% after 350 cycles, and a stable voltage fluctuation after cycling for 1000 h (Table 1).[80] This result verifies the contribution of single-atom Zn to inducing Na nucleation during the electrodeposition process. However, there is a need to further explore and understand why Zn atoms exhibit much lower nucleation barriers for Na compared to Li. These results provide us insights into the underlying mechanism controlling the Na nucleation behaviors, benefiting the atomic-level design of electrodes for Na metal anodes.

Indeed, it has been demonstrated that single-atom Zn sites show excellent capabilities in guiding the nucleation of Li and

https://doi.org/10.1021/acsnano.4c08831
ACS Nano 2024, 18, 25966−25985

Na. Hence, researchers are now exploring whether the single-atom sites could be further suitable for other metal anodes with similar results, such as Zn anodes. It is well-known that Zn anodes are still suffering from the uncontrollable formation of Zn dendrites, which limits the application of aqueous zinc-ion batteries. To address this challenge, Lee et al. fabricated a 3D N,O-codoped porous carbon with single-atom Cu sites (Cu-NOC) for Zn anodes.[85] A low nucleation overpotential of 28 mV was achieved at 2 mA cm^{-2} (Figure 4h), notably superior to that of N,O-codoped porous carbon (52 mV). DFT calculations revealed that N, O elements onto carbon could uniformly disperse Cu sites through the Cu-N-C and Cu-N-O configurations, creating sufficient zincophilic sites for stable Zn nucleation. Consequently, Cu-NOC demonstrates exceptional reversibility up to ∼800 h with a fixed Zn plating/stripping capacity of 5 mAh cm^{-2} (Table 1).[85] This good performance should be attributed to the 3D channel scaffold that benefits uniform Zn^{2+} flux, efficiently adjusting volume changes during cycles. This design contributes to the extended lifespan and enhanced reversibility of the Zn metal anodes. Similar phenomena have been observed by Prof. Yu et al. through the development of single Cu atoms in a leaf-like zinc-coordinated zeolitic imidazolate framework on Ti mesh (Cu-ZIF-Ti).[94] Due to the existence of zincophilic Cu atoms within the 3D conductive matrix, a lower Zn nucleation overpotential of ∼25 mV was also achieved at 1 mA cm^{-2} (Figure 4i), compared to that of Cu-NOC mentioned earlier. As anticipated, the resulting Cu-ZIF-Ti electrode demonstrated good Zn plating/stripping performance more than 1100 h at 1 mA cm^{-2} with a small potential polarization of ∼50 mV at room temperature (Table 1).[94] However, Zn nucleation encounters significant challenges, such as sluggish kinetics at subzero temperatures in aqueous zinc-ion batteries. Hence, it is highly desirable to explore whether single-atom sites could effectively function under these extreme conditions. In response to these issues, Wang et al. proposed the use of Bi atoms, which is highly active with maximum atom utilization to serve as a Zn nucleating agent.[83] Consequently, the single-atom Bi sites have shown effectiveness in promoting highly reversible zinc plating-stripping behaviors even at subzero temperatures. At a high current density of 5 mA cm^{-2}, an average CE of 99.4% over 1600 cycles is obtained at a low temperature of −30 °C. Additionally, low-temperature full cells exhibit a nearly 100% capacity retention after cycling at 0.5 A g^{-1} for 1400 cycles (Table 1).[83] This study underscores the feasibility of employing single atoms to manipulate nucleation behaviors, particularly in the context of low-temperature metal batteries.

3.2. Metallophilic Sites without Electrochemical Activity. As for metallophilic sites lacking electrochemical activity, they are unable to directly alloy with metals in metal-based anodes. However, these metallophilic sites can change the coordination environment and electronic structure of the substrate materials through specific bonding. The alteration of the local electronic structure can promote the absorption of metal ions and facilitate the subsequent metal nucleation. These metallophilic sites mainly include metal−nitrogen coordinations, such as Co-N_x,[91,92,95,96] Co-O_x,[97] Co-N_x/O_x,[87] Ni-N_x,[98] Fe-N_x,[99] or Mn-N_x[86] moieties. Thus, to investigate the nucleation characteristics of metal-N moieties in metal anodes, Prof. Zhang fabricated Co-N_x-doped graphene material as a Li host.[91] DFT calculations illustrated that the introduction of Co atoms significantly altered the local electronic structure, thereby enhancing the binding energy with Li atoms (Figure 5a and 5b). This enhancement enabled strong lithiophilicity, ensuring uniform lithium nucleation and deposition. Consequently, the battery delivers an exceptionally high CE exceeding 99% across various current densities and cycle numbers (Figure 5c).[91] Indeed, Co-N_x sites exhibit effective function of nucleating guidance across various metals (Li/K/NaK) as anchored on different hosts, including nitrogen−carbon nanosheet,[92] hollow carbon matrix,[95] or carbon nanoarrays.[96] For instance, Lu et al. introduced a low-tortuosity carbon structure adorned with single Co atoms (SA-Co@HC) to serve as a metal K host, effectively addressing dendrite growth issues.[95] The existence of Co sites on the N-doped carbonaceous matrix reduces nucleation energy barriers and enhances the kinetics of K deposition (Figure 5d and 5e). Additionally, the low-tortuosity structure modifies the electric field, facilitating the rapid transport of K ions. Consequently, the symmetric cell with SA-Co@HC/K anode exhibits dendrite-free K plating and stripping behavior, along with exceptional cycling stability exceeding 2500 h at 0.5 mA cm^{-2}.[95]

Despite the focus on Co-N_x coordination, researchers have also explored the Li nucleation properties of Co-O_x coordination. Prof. Wu and co-workers introduced single Co atoms on graphene via bonding with O species (CoSA-O-G) and applied it for Li plating.[97] In comparison to its N-coordinated counterparts, CoSA-O-G offers more uniform and abundant lithiophilic sites, enhanced electronic conductivity, and a larger specific surface area. Consequently, the Li anodes based on CoSA-O-G demonstrate a high CE, an excellent rate capability, and a prolonged cycling lifespan (Table 1). DFT calculations disclose a stronger interaction between CoSA-O-G and Li atoms compared to Co-N_x, facilitating uniform Li distribution (Figure 5f and 5g).[97] Since both Co-N_x and Co-O_x coordinations exhibit excellent performance in promoting Li nucleation, researchers are wondering whether the combination of the two coordination sites would have a better performance than the individual site. Based on this concept, a carbon-supported Co-atom nanocomposite with asymmetric N, O coordinations (Co-N/O) is fabricated.[87] Both experimental and theoretical analyses reveal that the uniformly dispersed Co atoms with asymmetric N and O coordination exhibit improved binding ability with Li atoms compared to N-coordinated or isolated O sites, facilitating uniform lithium plating and stripping (Figure 5h). Consequently, the lithium metal anodes exhibit superior electrochemical performance, including a uniform lithium deposition, an extended cycling life, and an excellent rate capability.[87]

The above results demonstrate that metal-N coordination having an improved binding energy should possess better Li plating/stripping properties. However, Gong et al. proposed a different viewpoint, and elaborated that the binding energy between metal-N moieties (Mn, Ni, Co, Zn, and Zr) and lithium should fall within a certain range that is sufficiently large to adsorb Li atoms and yet small enough to maintain structural stability.[86] Subsequently, they investigated various metal-N coordinations through both electrochemical experiments and theoretical calculations (Figure 5i). It is found that Mn-N_x coordination with moderate binding energy to Li atoms exhibit good electrochemical performance.[86] It is demonstrated that the binding energy to Li atoms should be in a certain threshold range to prevent the growth of dendrites. This

https://doi.org/10.1021/acsnano.4c08831
ACS Nano 2024, 18, 25966−25985

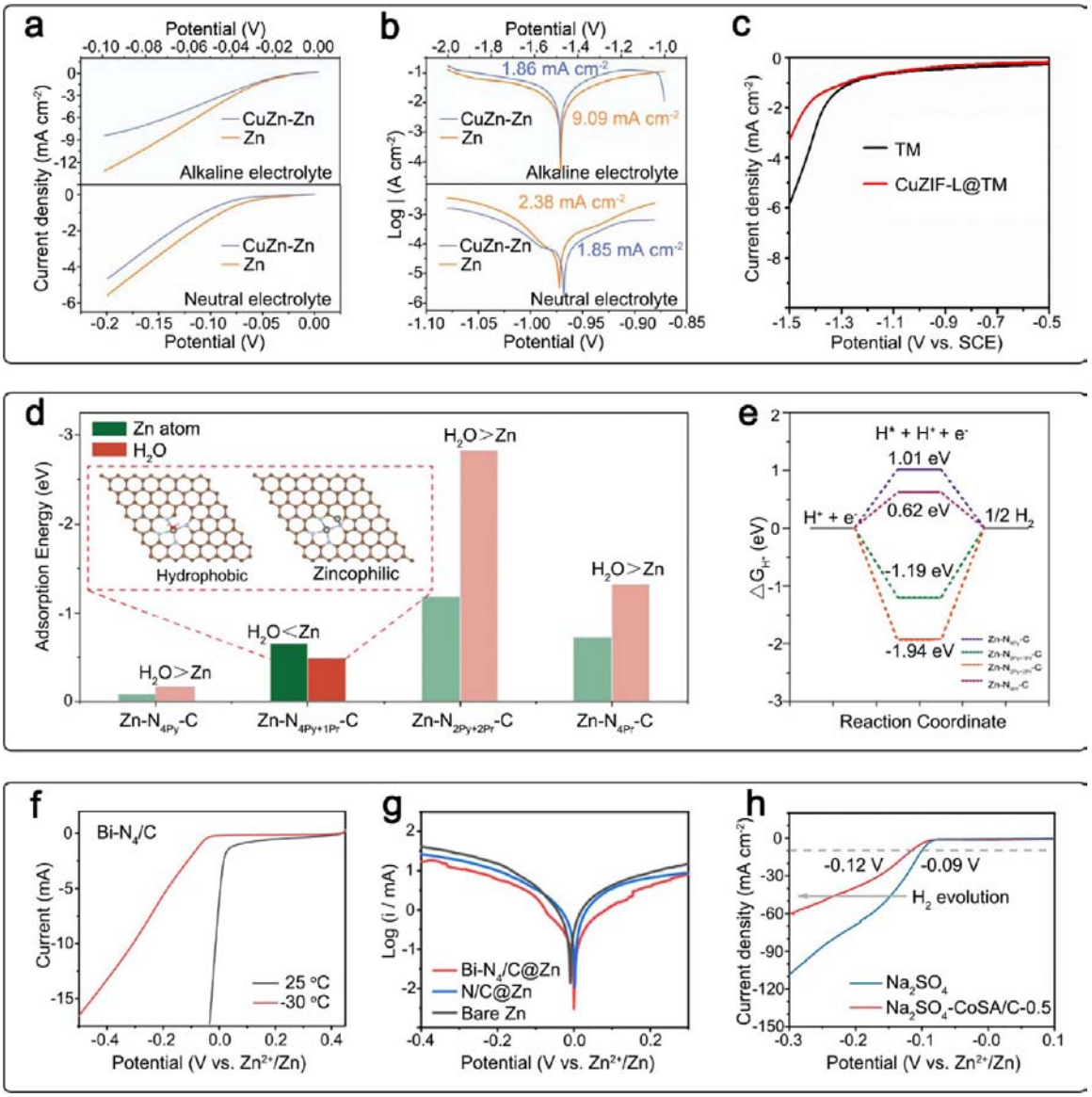

Figure 6. (a) The LSV curves and (b) corrosion curves of Zn and CuZn-Zn electrodes in alkaline and neutral electrolyte.[100] Reproduced with permission from ref 100. Copyright 2022 Wiley-VCH. (c) LSV curves of TM and CuZIF-L@TM for HER.[94] Reproduced with permission from ref 94. Copyright 2022 Wiley-VCH. (d) Calculated adsorption energy of H_2O molecule and Zn atom on the Zn-N_4-Cs. (e) H* free energy (ΔG_{H^*}) calculated on the Zn-N_4-Cs.[88] Reproduced with permission from ref 88. Copyright 2024 Wiley-VCH. (f) LSV curves of Bi-N_4/C electrode in aqueous electrolyte at 25 °C and −30 °C. (g) Tafel polarization curves in 2 M Zn $(OTF)_2$ aqueous solution at −30 °C.[83] Reproduced with permission from ref 83. Copyright 2022 American Chemical Society. (h) Hydrogen evolution polarization curves of Zn anode in the ZSO and ZSO-CoSA/C-0.5 electrolytes at 1 mV s^{-1}.[101] Reproduced with permission from ref 101. Copyright 2024 Wiley-VCH.

finding provides valuable insights for the development of lithium anodes.

HAIE effectively addresses dendrite formation and uneven metal deposition in metal anodes by introducing metallophilic sites for guiding uniform nucleation. This technique reduces nucleation barriers and enhances metal transfer kinetics using single-atom sites and optimized substrates. Notable advancements with Zn, Co, and other metals have significantly improved the battery stability and efficiency. However, whether single-atom sites continue to play a role in the subsequent stage of metal growth remains to be studied. Although the initial nucleation of crystals determines the subsequent growth state, the growth process is not always ideal. Crystal growth often leads to structural deformation or defects, introducing uncertainties into the subsequent growth stage. Therefore, the extent to which single-atom-induced nucleation influences later stage of crystal growth requires further investigation. If this issue is resolved, then HAIE would hold great promise for developing high-performance and dendrite-free metal anodes, which are essential for the progress of metal-based batteries.

4. HETEROATOM IMMOBILIZATION ENGINEERING TO INHIBIT SIDE REACTIONS AT THE METAL ANODE SURFACE

We further investigated how HAIE functions to inhibit side reactions in metal-based batteries. By incorporation of specific heteroatoms into the electrode materials or artificial SEI film, HAIE minimizes the unwanted chemical reactions that can degrade battery performance over time. Suppressing these side

https://doi.org/10.1021/acsnano.4c08831
ACS Nano 2024, 18, 25966−25985

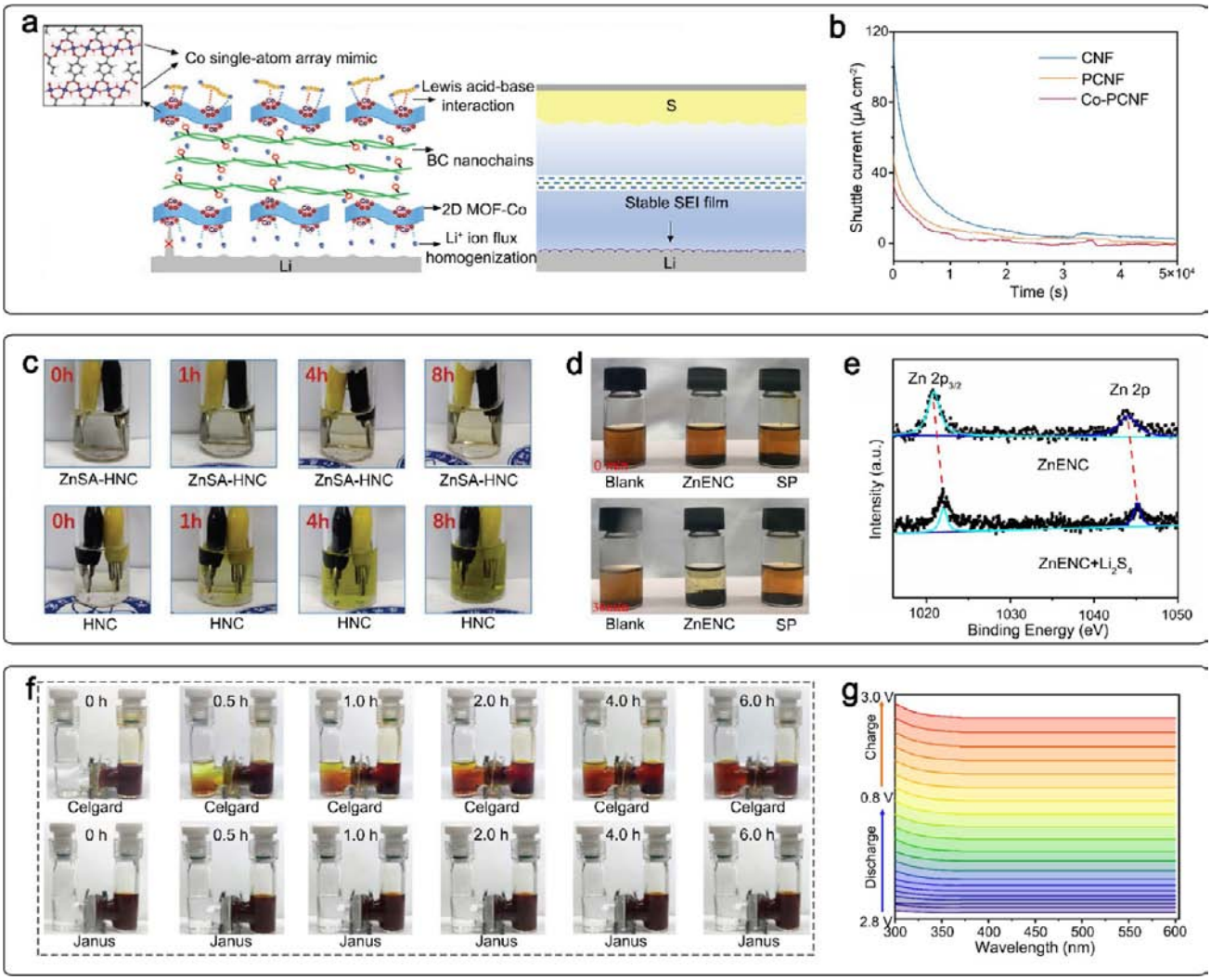

Figure 7. (a) Schematic illustration for the Li-S batteries with B/2D MOF-Co separators, in which numerous Co-O_4 moieties array on 2D MOF-Co nanosheets could anchor polysulfides via Lewis acid−base interaction and homogenize Li^+ ion flux, resulting in effective suppression of dendrites and polysulfide diffusion.[102] Reproduced with permission from ref 102. Copyright 2020 Wiley-VCH. (b) Shuttle current curves of Li-S batteries with S/Co-PCNF, S/PCNF, and S/CNF cathodes.[103] Reproduced with permission from ref 103. Copyright 2021 American Chemical Society. (c) Visual illustration of polysulfide entrapment at different discharge process by Zn1-HNC-S (top) and HNC-S (bottom) cathode-based Li-S batteries.[106] Reproduced with permission from ref 106. Copyright 2020 Wiley-VCH. (d) LiPSs adsorption tests for ZnENC and SP. (e) XPS Zn 2p spectra of ZnENC before and after adsorption of Li_2S_4.[82] Reproduced with permission from ref 82. Copyright 2021 American Chemical Society. (f) Visualization experiments of polysulfide blocking for the Celgard and the Janus-S.[108] Reproduced with permission from ref 108. Copyright 2022 Wiley-VCH. (g) *In situ* UV−vis spectra of S@SA Fe-N/S@CNF.[84] Reproduced with permission from ref 84. Copyright 2023 Wiley-VCH.

reactions improves cycling stability and enhances the overall efficiency of the battery system.

4.1. Inhibit Hydrogen Evolution Reaction (HER) in Aqueous Zinc-Ion Batteries. The large-scale applications of aqueous zinc-ion batteries are hindered by the Zn dendrite formation and also by side reactions including the hydrogen evolution reaction. This arises from the use of aqueous electrolytes with zinc metal anodes during cycling because the standard potential of Zn/Zn^{2+} is −0.76 V, lower than the hydrogen evolution potential (H^+/H_2, 0 V). Thus, hydrogen evolution should be unavoidable in theory. The hydrogen evolution reaction can gradually consume the electrolyte producing gas, resulting in swelling and failure of batteries. To inhibit hydrogen evolution, two strategies have been developed: artificial protective layers and electrolyte additives. As for artificial protective layers, researchers have turned their attention to selected metals that can decrease the practical potential for hydrogen evolution and inhibit the side reaction. These metals include Cu,[85,94,100] Bi,[83] and Co.[101] For instance, Lu et al. employed a CuZn alloy for the electrochemical deposition of Zn, capitalizing on the nonreactive nature of Cu toward the HER and the high dezincification potential of the CuZn alloy to significantly mitigate H_2 generation and Zn corrosion in aqueous electrolytes (Figure 6a and 6b).[100] Consequently, the symmetric cells utilizing CuZn-Zn electrodes demonstrated exceptional cycling life in both alkaline and neutral electrolytes, achieving stable operation for more than 800 h at 2.5 mAh cm^{-2}, superior to initial zinc anodes.[100] This research provides the utilization of inert metals toward mitigating the HER in both alkaline and neutral electrolytes.

However, the excessive usage of a CuZn alloy, with a high proportion of Cu metal in the anodes, can significantly

https://doi.org/10.1021/acsnano.4c08831
ACS Nano 2024, 18, 25966−25985

decrease the energy density of the entire zinc-ion batteries. Therefore, it is important to reduce the consumption of metals while simultaneously inhibiting the HER. In this regard, HAIE offers significant advantages due to their minimal usage of inner metals. Thus, a Cu-ZIF-Ti electrode, as proposed by Yu et al., was employed to investigate its HER property through linear sweep voltammetry (LSV) measurements.[94] In Figure 6c, Cu-ZIF-Ti demonstrates a lower HER activity than that of ZIF-Ti, indicating that the single-atom Cu sites could effectively suppress the HER property in Zn-ion batteries. Consequently, a full cell assembled with the Cu-ZIF-Ti-Zn anode exhibits a stable cycling performance over 1000 cycles (Table 1).[94] Similarly, atomically dispersed Cu sites on N,O-codoped carbon hosts have demonstrated good electrochemical performance. The full cell with Cu-NOC-Zn anodes and V_2O_5 cathode shows an excellent rate property up to 5 A g^{-1} and a long cycles more than 400 times at 0.5 A g^{-1} (Table 1).[85]

Besides, other metal-N_x coordinations such as Zn-N_4,[88] Bi-N_4,[83] and Co-N_3[101] also function to inhibit hydrogen evolution on the surface of Zn anodes. For instance, Prof. Liu and his co-workers proposed a zincophobic/hydrophilic carbon nanomaterial containing Zn-N_4 configuration (Zn-N_4-C) to inhibit the HER and protect Zn anodes.[88] Theoretical investigations reveal that Zn-N_4-C could inhibit the HER as characterized by the enhanced H* free energy (ΔG_{H^*}) (Figure 6d and 6e). Consequently, the symmetric cells with the Zn-N_4-C-Zn anode exhibit a cycling performance of 500 h at a depth of discharge up to 50%, and the corresponding full cell shows a long cyclic life up to 1000 cycles at 10 A g^{-1}.[88] This strategy of constructing zincophilic/hydrophobic metal-N-C materials holds great promise for inhibiting HER in zinc-ion batteries. Additionally, Wang et al. adopted a strategy of indirectly suppress HER by adjusting the operating temperature of Zn-ion batteries to low temperatures.[83] In the low-temperature range, both Zn plating/stripping kinetics and HER activity could be significantly reduced (Figure 6f). Thus, the Bi-N_4 moieties were utilized to accelerate the Zn plating/stripping kinetics at low temperatures, without promoting the HER kinetics (Figure 6g). As a result, the low-temperature full cells exhibited a high capacity retention nearly 100% after cycling at 0.5 A g^{-1} for 1400 cycles.[83]

In addition to constructing of protective layer, single-atom sites also exhibit effective functions in the electrolyte additives to suppress the HER. Recently, Yu et al. introduced trace amounts of Co single atoms anchored on carbon (CoSA/C) as an electrolyte additive to inhibit the HER at the Zn−electrolyte interface.[101] The hydrogen evolution polarization curves (Figure 6h) show that the Na_2SO_4 electrolyte with the CoSA/C additive exhibits a low current density in the HER, indicating the suppressed HER performance. Meanwhile, the atomically dispersed Co-N_3 sites can redistribute the space electric field and regulate ion flux, promoting homogeneous zinc plating. Consequently, the Zn||Zn symmetric cell with CoSA/C additive demonstrates a stable cyclic life more than 1600 h at 10 mA cm^{-2}.[101] This study provides a simple electrolyte-additive strategy to inhibit HER in aqueous Zn-ion batteries and holds great potential for its applications in other aqueous-based batteries.

4.2. Inhibit the Electrolyte Consumption and Polysulfide Shuttle in Li-S Batteries. The growth of Li dendrites and the shuttle effect of polysulfides present significant challenges to the advancement of Li-S batteries. Lithium dendrites are formed because of inhomogeneous Li stripping-plating at the surface of the anode, which exposes a highly active surface for irreversible side reactions with the electrolyte. This leads to substantial electrolyte consumption and subsequent increases in the internal resistance. Indeed, addressing the dendrite growth issue can have a positive impact on reducing the consumption of electrolytes. As previously discussed, single-atom metal sites can effectively lower lithium nucleation barriers and benefit uniform Li growth, offering a promising strategy to mitigate dendrite formation and improve battery performance. Additionally, single atoms play an important role in preventing the polysulfide shuttle at the separator by strongly adsorbing polysulfides, thereby inhibiting their migration to the surface of metal anodes. For example, Guo and his co-workers incorporated a bifunctional separator consisted of ultrathin metal organic framework (MOF) nanosheets with uniform Co elements coordinated with O atoms.[102] This "single atom array mimic" could not only evenly distribute the Li ion flux, stabilizing Li stripping/plating at the anode side, but also function as "traps" to mitigate the movement of polysulfide species characterized by Lewis acid−base interactions (Figure 7a). Consequently, the full cells with this bifunctional separator exhibited an extended cyclic stability with a low capacity loss of 0.07% per cycle more than 600 times and maintained a good reversible areal capacity of 5.0 mAh cm^{-2} after 200 cycles, with a high S loading of ∼8.0 mg cm^{-2}.[102] Besides, Prof. Sun and co-workers introduced a dual-functional fibrous skeleton implanted with atomically dispersed Co-N_x coordination to adjust both anode and separator simultaneously.[103] The integration of single-atom Co-N_x sites improves the bidirectional conversion kinetics of S and effectively inhibits the shuttle effect of polysulfides. Shuttle currents were detected to evaluate the inhabitation behavior for the shuttle effect (Figure 7b). Notably, the cathode with the Co-N_x configuration shows the smallest shuttle current compared to all the examined electrodes, demonstrating its advanced polysulfide trapping ability. Benefiting from the synergistic effects between single-atom Co-N_x sites and the conductive network, the full cells deliver a high reversible areal capacity (>7.0 mAh cm^{-2}) at a S loading of 6.9 mg cm^{-2}.[103] The dual functionality highlights the potential of single-atom sites in enhancing the stability and efficiency of Li-S batteries. Similar results were also achieved by Lin et al., who established a conductive network by confining single Co atoms within defect-containing iron sulfide nanoparticles in S-doped conductive nanocarbon.[104] This hybrid host facilitates the catalytic effects on lithium ion kinetics, promoting uniform nucleation and deposition with reduced barriers. Consequently, a Li/S pouch cell with this hybrid host shows promising electrochemical performance, indicating the potential for practical applications. Moreover, Co and Fe bimetallic atoms (Co/Fe-SA) are incorporated into a 3D dodecahedral material ZIF-8 to construct a functional modified separator, as reported by Li et al.[105] This separator effectively suppresses the shuttle effect of LiPSs owing to the synergistic effect of Co/Fe-SA. Consequently, Li-S batteries with the Co/Fe-SA separator deliver a specific discharge capacity of 1404 mAh g^{-1} at 0.1 C and a stable cycle. Even after 500 cycles at 1 C, a specific discharge capacity of 541 mAh g^{-1} with a capacity decay rate of 0.08% per cycle and a stable CE of over 98% are achieved.[105]

Other metal-N_x coordinations such as Zn-N_x,[82,106] Mo-N_x,[107] and Ru-N_x[108] also exhibit good adsorption properties

https://doi.org/10.1021/acsnano.4c08831
ACS Nano 2024, 18, 25966−25985

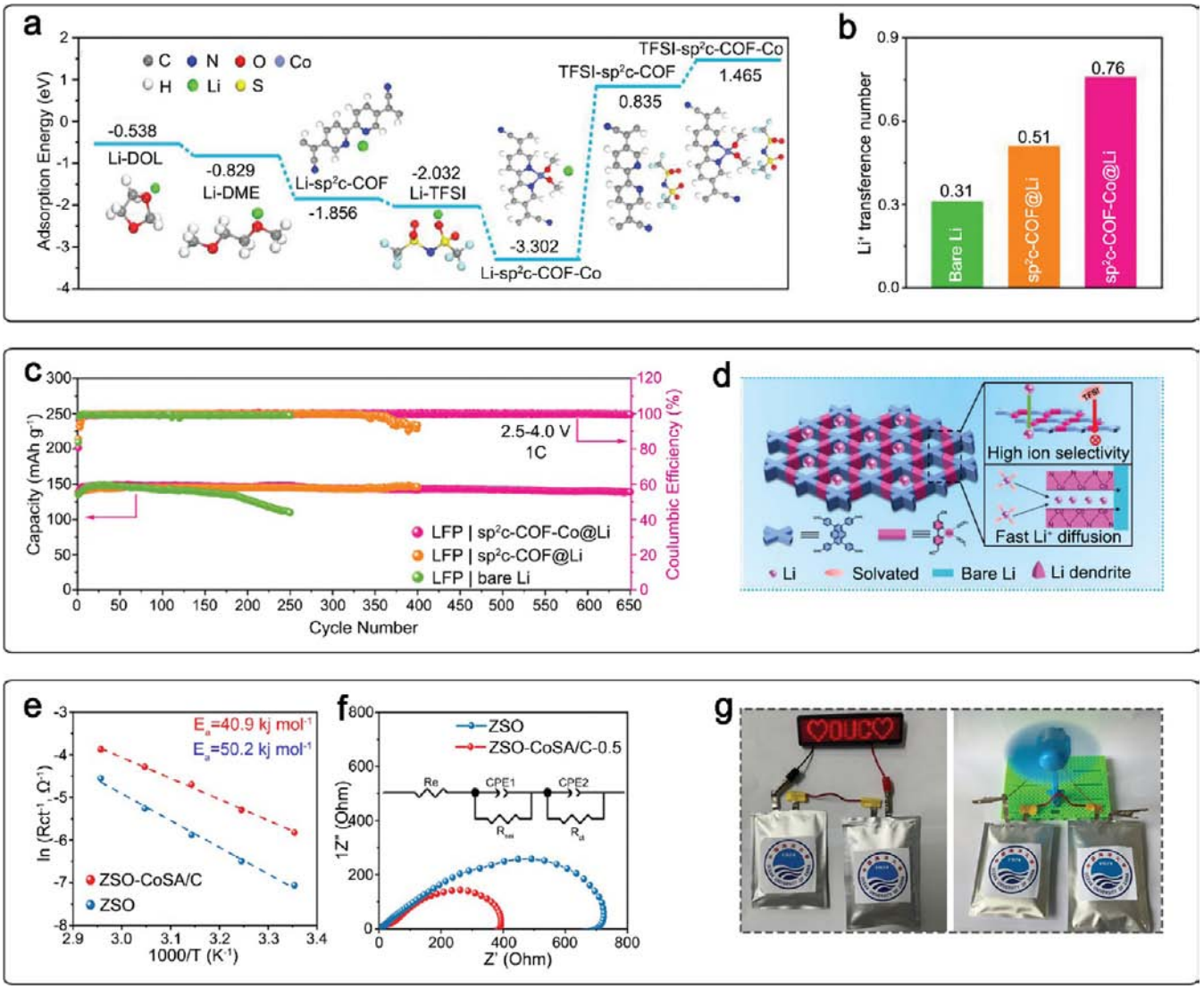

Figure 8. (a) Chemical coordination circumstance of simulated affinity energy between COFs (sp^2c-COF and sp^2c-COF-Co) fragment and LiTFSI-based electrolyte with the terminal optimized geometries. (b) Li^+ transfer number of bare Li, sp^2c-COF@Li and sp^2c-COF-Co@Li (c) Long-term cycling performances of LFP, LCO and NCM full cells at 1.0 C. (d) Mechanism of the deposition processes for sp^2c-COF-Co@Li and bare Li surfaces.[89] Reproduced with permission from ref 89. Copyright 2023 Wiley-VCH. (e) Arrhenius behavior of temperature-dependent reciprocal resistances of Zn anode in ZSO and ZSO-CoSA/C-0.5 electrolytes. (f) Nyquist plots of Zn||Zn cells of Zn||Cu cells at a scan rate of 0.5 mV s^{-1} using ZSO and ZSO-CoSA/C-0.5 electrolytes. (g) Photographs of a LED plate and a fan powered by two pouch cells in series.[101] Reproduced with permission from ref 101. Copyright 2024 Wiley-VCH.

for LiPSs. For example, Prof. Wu and his co-workers introduced Zn atoms decorated carbon spheres (ZnSA-HNC) as dual-functional nanoreactors for inhibiting LiPSs shuttle.[106] The strong surface affinity of ZnSA-HNC for LiPSs was directly evidenced by *in situ* visual experiments (Figure 7c). A swift transformation from a transparent to a yellowish electrolyte occurs within an hour due to the surplus of LiPSs from the HNC-S electrode, contrasting sharply with the continued clarity of the electrolyte near the ZnSA-HNC-S cathode even after eight h, highlighting the strong immobilization effect of ZnSA-HNC on LiPSs. Consequently, the assembled full batteries demonstrate impressive electrochemical performances, including a long cycle stability with minimal capacity decay and a superb rate capability. Furthermore, a high areal capacity is achieved with a low electrolyte-to-S ratio, highlighting the potential of ZnSA-HNC nanoreactors for high-energy-density Li-S batteries.[106] Lan et al. also constructed that Zn-N_x coordinations can effectively inhibit the shuttle of LiPSs.[82] The adsorption test and XPS spectra (Figure 7d and 7e) both show a strong interaction between Zn atoms and polysulfides. With the utilization of a Zn-N_x separator, the full cell shows a stable cyclic performance and an excellent cyclic stability in Li-S batteries.[82] Additionally, Xiong et al. demonstrated that there was not obvious color change in the blank side of Mo/NG@PP enabled by Mo-N_x sites, while a distinct color change appeared in NG@PP and deepened further in pure PP.[107] This observation indicates that Mo-N_x sites exhibit excellent inhibition of the shuttle effect. Similar results have also been obtained with Ru-N_x sites.[108] The migration flux of polysulfides in electrolytes determines the magnitude of the shuttle current. In LSBs with a Janus-S, the shuttle current is only ~1.7×10^{-2} mA, lowest among the three battery configurations (Figure 7f).[108]

https://doi.org/10.1021/acsnano.4c08831
ACS Nano 2024, 18, 25966−25985

In addition to inhibiting LiPSs, metal-N_x coordinations (Fe-N_x,[84] Y-N_x,[109] and Ni-N_x) also exhibit strong affinity for other polysulfides or polyselenides. For instance, Yu et al. synthesized single Fe-N/S active centers by controlling the second-shell coordinating environment of Fe atoms (SA Fe-N/S@CNF).[84] *In situ* ultraviolet−visible spectra demonstrated the inexistence of polysulfides in the electrolytes enabled by S@SA Fe-N/S@CNF cathode, significantly inhibiting the shuttle effect in the room-temperature Na-S system (Figure 7g). The Fe-N_4S_2 coordination enhanced the local electron density around the Fermi level, thereby promoting the transformation kinetics of polysulfides. Consequently, a high reversible capacity of 1590 mAh g^{-1} was obtained in the first cycle, which is nearly 95% of the theoretical capacity. Moreover, the assembled Na-S pouch cell exhibited a high energy density of 657.1 Wh kg^{-1}, underscoring its promising application potential.[84] Besides, Li and his colleagues demonstrated that the incorporation of Y-N_x can effectively prevent the shuttle effect of polysulfides. In their study, the electrolyte remained colorless in the Y-N_x/NC-S cell after discharging for 16 h, while it turned slightly pale yellow just after 2 h in the NC-S cell.[109] Similar to the shuttle effect of polysulfides, polyselenides also pose challenges in metal-selenium batteries. To address this challenge, Rogach et al. proposed the utilization of Ni-N_x sites in carbon-based materials.[110] The Na-Se battery demonstrated an excellent cycle stability and an improved safety.[110] This innovative approach is promising for the practical application of Na-Se batteries.

HAIE reduces side reactions in metal-based batteries by incorporating specific heteroatoms into electrode materials or artificial SEI films. This technique enhances the cycling stability and overall efficiency. In aqueous zinc-ion batteries, HAIE strategies, such as protective layers and electrolyte additives, effectively inhibit the HER. In Li-S batteries, single-atom sites help prevent lithium dendrite formation and the polysulfide shuttle effect, leading to improved performance. However, while single-atom sites could inhibit hydrogen evolution and obstruct the polysulfide shuttle effect, they may also introduce other undesirable side reactions such as the OER or the decomposition of organic electrolytes. Therefore, it is crucial to balance the benefits and drawbacks of different reactions by selecting appropriate single-atom materials. If the various reactions can be quantitatively assessed, then HAIE also shows promise in addressing similar issues in Na-S and Na-Se batteries, making it a versatile approach for various battery technologies.

5. HETEROATOM IMMOBILIZATION ENGINEERING TO PROMOTE DESOLVATION OF METAL IONS AT THE ELECTRODE/ELECTROLYTE INTERFACE

We explore the role of HAIE in promoting the desolvation of metal ions and accelerating the reaction kinetics in metal-based batteries. Through precise immobilization of heteroatoms, HAIE could modify the solvation environment around metal ions, facilitating their rapid desolvation and subsequent plating on the metal anode during battery operation. The improved desolvation process can enhance the overall efficiency of metal-ion transport within the battery system, leading to improved charge/discharge rates and enhanced energy storage capabilities.

To address the issue of Li^+ desolvation, Prof. Guo et al. proposed the incorporation of single Co atoms within the sp^2c-COF structure.[89] DFT calculations disclose that the interaction force between Li^+ and sp^2c-COF-Co was −3.302 eV (Figure 8a), surpassing other solvents such as Li-DOL (0.538 eV), Li-DME (−0.829 eV), Li-sp^2c-COF (−1.856 eV), or Li-TFSI (−2.032 eV), favoring Li^+ desolvation from solvent clusters. Additionally, the binding energy of $TFSI^-$ and COFs was assessed. Specifically, the adsorption energy of TFSI-sp^2c-COF-Co was 1.465 eV, lower than that of TFSI-sp^2c-COF (0.835 eV), indicating the capability of sp^2c-COF-Co to repel $TFSI^-$ anions. The synergistic effect of the improved desolvation and repulsion of anions by sp^2c-COF-Co enhances the migration kinetics of Li^+, leading to a high Li^+ transfer number of 0.76 (Figure 8b). Furthermore, sp^2c-COF-Co-based full cells demonstrate an extended cycle life with a high-capacity retention (Figure 8c), indicating the potential of this approach for practical applications in Li-metal batteries. This is attributed to both desolvation of Li^+ and repulsion of $TFSI^-$ enabled by Co single atoms within the COF structure, benefiting electron transfer to COF and strengthening the electron density (Figure 8d).[89]

Single-atom metal sites are also highly effective to benefit the desolvation of Zn^{2+} in aqueous zinc-ion batteries. For instance, Yu et al. confirmed the effectiveness of Co-N_3 sites via calculating the activation energy.[101] The process of desolvation for hydrated zinc ions (Zn^{2+}) in a range of electrolytes was systematically evaluated by quantitatively determining the activation energy (E_a) using the Arrhenius equation. The calculated E_a value for the ZSO-CoSA/C-0.5 electrolyte is 40.90 kJ mol^{-1} (Figure 8e), lower than that for the ZSO electrolyte (52.20 kJ mol^{-1}), indicating the enhanced desolvation process by the CoSA/C additive. Besides, the Zn anode in the ZSO-CoSA/C-0.5 electrolyte exhibits a smaller R_{ct} than that in the ZSO electrolyte at all temperatures (Figure 8f), confirming more rapid charge transfer at the interface. Consequently, the Zn||V_2O_5 batteries with CoSA/C additive was fabricated and demonstrated good cyclic life. Moreover, no obvious gas release was observed in the aforementioned pouch cells after cycling, further affirming their stability.[101]

HAIE could enhance the desolvation of metal ions, improving reaction kinetics in metal-based batteries. By precisely immobilizing heteroatoms, HAIE modifies the solvation environment, facilitating rapid desolvation and plating of metal ions on the anode. This process could accelerate metal-ion transport, boosting charge/discharge rates, and energy storage. However, further studies are still needed to investigate whether single-atom sites can effectively function in various solvation environments. The solvation environment is dynamic and can change with external factors, such as temperature, pressure, or charging/discharging conditions. In particular, under low-temperature conditions where metal ion desolvation and reaction kinetics are sluggish, the extent to that single atoms can enhance desolvation and improve reaction kinetics remains uncertain, providing broad research horizons for further investigation.

6. STRATEGIES FOR HETEROATOM IMMOBILIZATION ENGINEERING TO FABRICATE SINGLE-ATOM METAL SITES

We discuss various strategies for implementing HAIE in electrode materials, including the selection of appropriate heteroatoms, optimization of immobilization methods, and construction of materials architectures. These strategies aim to optimize performance and enhance capabilities of HAIE,

https://doi.org/10.1021/acsnano.4c08831
ACS Nano 2024, 18, 25966−25985

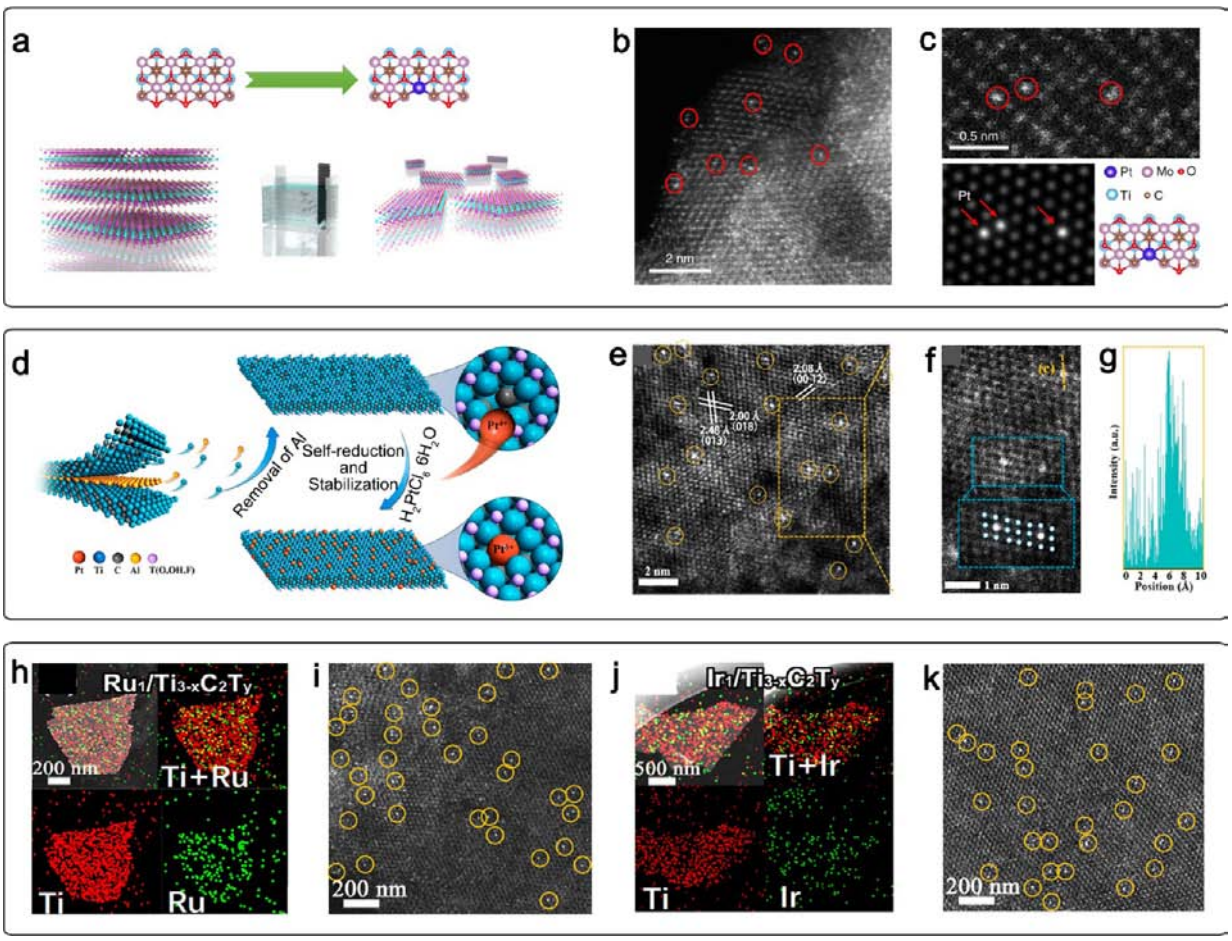

Figure 9. (a) Schematic illustration of the electrochemical exfoliation process of MXene to immobilize single Pt atoms. (b) HAADF-STEM image of $Mo_2TiC_2T_x$-PtSA. (c) Magnified HAADF-STEM image of $Mo_2TiC_2T_x$-PtSA, corresponding simulated image and illustration of the structure of $Mo_2TiC_2T_x$-PtSA, showing the presence of isolated Pt atoms (circles in b and c).[112] Reproduced with permission from ref 112. Copyright 2018 Nature Publishing Group. (d) Illustration of the simultaneous self-reduction-stabilization process for the preparation of $Pt_1/Ti_{3-x}C_2T_y$. (e) HAADF-STEM image of $Pt_1/Ti_{3-x}C_2T_y$. (f) Magnified HAADF image of the area in the yellow dashed box in (e). Inset is the corresponding atomic model. (g) Line intensity profile along the dashed line in (f). HAADF-STEM and corresponding element mapping images, showing distributions of Ti (red) and metal (green): (h, i) Ru and (j, k) Ir, respectively.[113] Reproduced with permission from ref 113. Copyright 2019 American Chemical Society.

thereby facilitating its widespread application in next-generation metal-based battery technologies. Recent literature has reported a wide range of experimental techniques for the preparation of single-atom materials. These techniques include high-temperature pyrolysis,[86,87,97,99] vacancy reduction,[111−113] and molten-salt etching and anchoring.[81,114−118]

6.1. High-Temperature Pyrolysis. Several pyrolysis methods have been employed to prepare single-atom materials. For instance, a common method involves hydrothermal treatment of GO solutions with metal salts, forming hybrids of carbon matrices and metal complexes to produce metal-ion-containing porous hydrogels.[86,87,97] Then, these hydrogels are annealed in an NH_3 or Ar atmosphere to obtain carbon-based single-atom materials. This method fascinates the formation of metal-atom moieties, such as M-N_4, embedded within the lattice of graphene. Besides, MOFs or ZIFs have garnered interest because of their precisely defined porous structure and organized configuration of organic linkers and metal nodes.[82,92,94] Through the pyrolysis of MOFs or ZIFs, single metal atoms can be obtained and incorporated into a carbon matrix. Additionally, polymer precursors have also been explored as an alternative method to synthesize single-atom materials.[98,99] By carbonizing polymer precursors, single-atom materials can be formed with a homogeneous distribution.

6.2. Vacancy Reduction. In recent studies on 2D MXene, an approach leveraging the reducibility of vacancies on the surface of MXene has been proposed for synthesizing single-atom materials.[112,113] For instance, atomically dispersed Pt atoms were anchored onto MXene layers by leveraging Mo vacancies through an electrochemical exfoliation process (Figure 9a).[112] In this complex process, the initially loosely packed $Mo_2TiC_2T_x$ underwent an exfoliation process, leading to its transformation into thin MXene nanosheets. Simultaneously, vacancies of molybdenum (V_{Mo}) appeared on the surfaces of these newly formed nanosheets. Meanwhile, platinum atoms from the counter electrode, which was a platinum foil, dissolved into the electrolyte solution. These Pt atoms were then captured by the available V_{Mo} (Figure 9b).[112] Owing to the high reducibility of V_{Mo}, the Pt ions underwent reduction at the V_{Mo} sites, forming single-atom Pt stabilized by the establishment of covalent Pt−C bonds on the $Mo_2TiC_2T_x$.[112] Building upon this groundwork, Chen further advanced this strategy by implementing a straightforward immersion method of metal salts in an aqueous solution. This

https://doi.org/10.1021/acsnano.4c08831
ACS Nano 2024, 18, 25966−25985

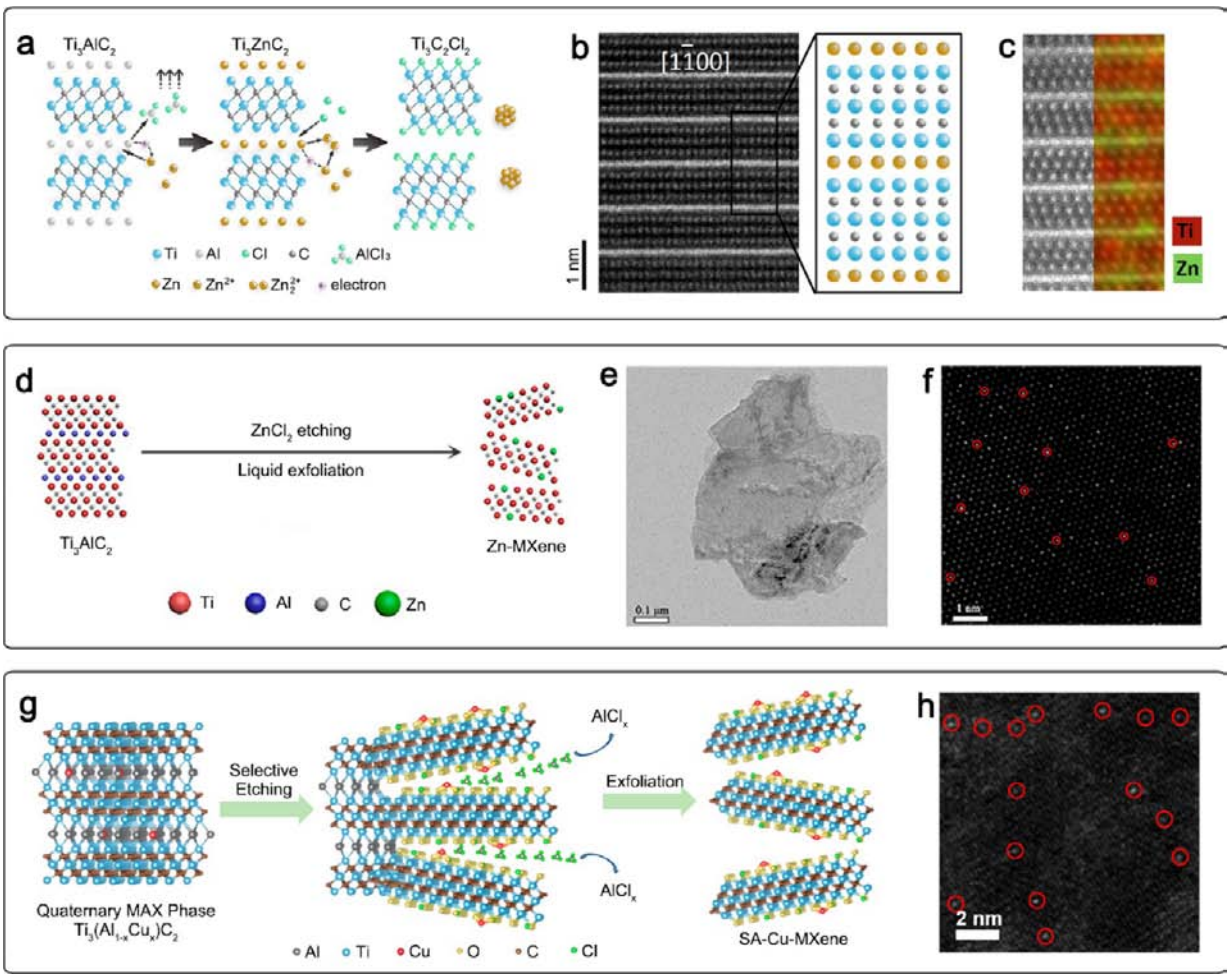

Figure 10. (a) Schematic illustration of the fabrication of Ti_3ZnC_2 and $Ti_3C_2Cl_2$ via molten-salt etching strategy. (b) STEM image of Ti_3ZnC_2, showing the atomic positions from different orientations. (c) STEM and the corresponding EDS mapping images of Ti_3ZnC_2.[120] Reproduced with permission from ref 120. Copyright 2019 American Chemical Society. (d) Synthesis process of single Zn atoms immobilized on MXene layers (Zn-MXene). (e) TEM and (f) HAADF-STEM images of Zn-MXene layer.[81] Reproduced with permission from ref 81. Copyright 2020 American Chemical Society. (g) Schematic illustration of the fabrication of SA-Cu-MXene via selective etching quaternary MAX-$Ti_3(Al_{1-x}Cu_x)C_2$, where gray, blue, red, yellow, brown, and green balls represent Al, Ti, Cu, O, C, and Cl atoms, respectively. (h) HAADF-STEM image of SA-Cu-MXene, showing the large presence of atomically isolated Cu atoms on the surface of MXene layers, which are marked with red circles.[114] Reproduced with permission from ref 81. Copyright 2021 American Chemical Society.

modification enabled the synthesis of a series of MXene-based single-atom materials, including Ru-$Ti_3C_2T_x$, Ir-$Ti_3C_2T_x$, Rh-$Ti_3C_2T_x$, and Pd-$Ti_3C_2T_x$ (Figure 9c–f).[113] In this approach, Ti vacancies were generated in $Ti_3C_2T_x$ MXene through the etching process conducted in a LiF and aqueous HCl system, which could be further confirmed by the HAADF-STEM images. Subsequently, as metal salt solutions were introduced into the MXene solution with magnetic stirring, the metal ions were homogeneously adsorbed onto the surface of $Ti_3C_2T_x$ flakes. These metal ions underwent gradual reduction by the highly reactive and reductive Ti vacancies, ultimately achieving stabilization on the MXene surface. By harnessing this strategy, the adsorption and reduction of single metal atoms occurred simultaneously, providing protection to the catalyst from the potentially harsh calcination reactions during multistep synthesis processes.[113]

6.3. Molten-Salt Etching and Anchoring. The molten-salt etching and anchoring strategy was initially proposed by Prof. Yang and his research team to facilitate the synthesis of single-atom Zn immobilized MXenes (Figure 10a).[81,119] This innovative approach was inspired based on the methodology established by Prof. Huang for producing both $Ti_3C_2Cl_2$-MXene and Ti_3ZnC_2-MAX materials through molten-salt etching method.[120] Prolonging the etching process allows single Zn atoms to effectively substitute Ti atoms within the metallic layer, resulting in the uniform dispersion of Zn atoms (Figure 10b and 10c). This is attributed to the drastic molten-salt reaction that occurs at high temperatures, leading to a substantial increase in metal vacancies and the subsequent reduction of highly reactive Zn atoms at these vacancies. This technique presents notable advantages in the synthesis of metal single atoms on MXene substrates, showing paramount significance in the realm of MXene-based single-atom materials. Besides, this strategy has been further used to produce single-atom Cu-$Ti_3C_2T_x$,[114] Co-Ti_2NT_x,[116] and Ni-Ti_3CNT_x,[117] broadening its utility and influence within the field. Associated with the development of MXene-based single-atom materials, advanced techniques, such as synchrotron-based X-ray absorption near-edge structure and extended X-ray absorption fine structure analyses, were conducted to investigate the coordination environment of the Cu atoms in Cu-$Ti_3C_2T_x$ (Figure 10d–f). These inquiries unveiled the

https://doi.org/10.1021/acsnano.4c08831
ACS Nano 2024, 18, 25966–25985

interplay between the Cu and O atoms on the MXene surface. Significantly, the fitting outcomes disclosed that the Cu atom on the SA-Cu-MXene showcased coordination with three O atoms, featuring a coordination number of 3.2 ± 0.4 and a bond length of 1.92 ± 0.02 Å.[114]

These strategies aim to optimize performance and enhance the capabilities of HAIE, benefiting its widespread application in next-generation metal-based battery technologies. In this regard, a series of experimental techniques such as high-temperature pyrolysis, vacancy reduction, and molten-salt etching and anchoring have been developed to prepare single-atom materials. High-temperature pyrolysis involves the annealing of metal-ion-containing hydrogels or MOFs/ZIFs in specific atmospheres to create single-atom materials. Vacancy reduction leverages the reducibility of vacancies on substrate surfaces like MXene to anchor single atoms, while molten-salt etching and anchoring utilize high-temperature reactions to substitute and uniformly disperse metal atoms within MXene layers. Consequently, advanced characterization techniques have been employed to investigate these materials, revealing detailed insights into their coordination environments and enhancing the understanding of their electrochemical properties.

7. CONCLUSIONS AND PERSPECTIVES

In conclusion, this review focuses on the fundamental principles of heterogeneous atom immobilization engineering in metal-based anodes and their significant role in enhancing battery performance. HAIE aims to tailor the atomic structure and surface properties of the anode material, optimizing its electrochemical performance. Specifically, we have explored how HAIE facilitates uniform nucleation in metal anodes by promoting the homogeneous nucleation of metal ions during charging and discharging cycles. Additionally, HAIE enables the inhibition of side reactions at the anode−electrolyte interface, minimizing unwanted chemical reactions that degrade battery performance. Moreover, we have investigated how HAIE promotes the desolvation of metal ions and accelerates reaction kinetics within metal-based batteries by modifying the solvation environment around metal ions.

Moving forward, various strategies for implementing HAIE in electrode materials have been discussed, including the selection of appropriate heteroatoms, optimization of immobilization methods, and exploration of materials architectures. These strategies aim to further refine the performance-enhancing capabilities of HAIE and facilitate its widespread application in next-generation metal-based battery technologies. However, despite the promising potential of HAIE, there are still some issues that need to be solved:

1) One challenge is to develop scalable and cost-effective methods for the synthesis and incorporation of heteroatoms into electrode materials. Currently, the reported approaches often involve complex and expensive techniques, limiting their practical applicability on a large scale. One key issue is the complexity and expense associated with current synthesis techniques. Many existing methods rely on intricate procedures and specialized equipment, which can inevitably increase the production costs and hinder the large-scale implementation. For instance, some techniques such as vacancy reduction often requires precise control over the synthesis process, making them impractical for mass production. Moreover, the involvement of high-temperature and high-pressure conditions also pose challenges, leading to batch-to-batch variability or inconsistent product quality. The synthesis of heteroatom-modified electrode materials involves multiple steps and intricate chemical reactions, further increasing the complexity and cost. For example, carbon-based materials doped with heteroatoms like Zn or Co typically involve the synthesis of precursors, followed by high-temperature treatments or chemical reactions to introduce the heteroatoms into the material structure.

   Addressing these challenges requires the development of synthesis strategies that are both scalable and cost-effective. This could facilitate the exploration of alternative synthesis routes that are simpler, more efficient, and less resource-intensive. For instance, advancements in materials science and nanotechnology may enable the development of innovative synthesis approaches that leverage bottom-up assembly or self-assembly processes to create heteroatom-modified electrode materials with precise control over structure and composition. Thus, overcoming the synthesis challenges and incorporate heteroatoms into electrode materials on a scalable and cost-effective basis is essential for realizing the full potential of HAIE in advancing next-generation metal-based battery technologies. Continued research and development in this area is crucial to drive the progress toward more sustainable and commercially viable battery systems.
2) Another significant challenge is the lack of comprehensive understanding regarding the function mechanism between heteroatoms and metal ions in metal-based batteries. While heteroatom immobilization engineering is promising to enhance the battery performance, the precise mechanisms governing these interactions remain unclear. Without a deep understanding of these mechanisms at the atomic level, it is challenging to optimize the design of heteroatom-modified electrode materials for improved battery performance.

   To address this challenge, exhaustive research is needed to unravel the underlying mechanism of the interactions between heteroatoms and metal ions. Advanced *in situ* characterization methods, including HAADF-STEM, electron microscopy, X-ray diffraction, and spectroscopic techniques, can provide insights into the structural evolution and degradation of heteroatom-modified electrodes during cycling. By systematically studying the morphological and chemical composition changes in the electrode materials over extended cycling periods, researchers can develop specific strategies to enhance their stability and reliability. Furthermore, computational modeling and simulation studies can complement experimental efforts by predicting the behavior of heteroatom-modified electrodes under various operating conditions. By studying these interactions under various operating conditions, researchers can elucidate how heteroatoms influence key electrochemical processes, such as ion diffusion, charge transfer, and surface reactions. These approaches can help optimize electrode design parameters, such as heteroatom concentration and distribution, to maximize performance and durability.

https://doi.org/10.1021/acsnano.4c08831
ACS Nano 2024, 18, 25966−25985

3) Moreover, the compatibility of HAIE with other battery components, such as electrolytes and separators, needs to be carefully considered to avoid detrimental effects on overall battery performance and safety. The compatibility issues are raised due to the interactions between heteroatoms and electrolyte components, as well as potential changes in the interface properties between the electrode and separator. One significant concern is the impact of heteroatoms on electrolyte stability and reactivity. Some heteroatoms may react with electrolyte components, leading to side reactions, electrolyte degradation, or the formation of unstable SEI films. These issues can compromise battery performance, reduce cycling stability, and pose safety risks, such as electrolyte decomposition or gas evolution.

To address these compatible challenges, several strategies have been developed. First, the careful selection of heteroatoms and incorporation methods is crucial to minimize adverse interactions with electrolytes. Heteroatoms with inherent stability and inertness toward electrolyte components should be prioritized. Moreover, the composition and formulation of electrolytes should be further optimized to enhance their compatibility with heteroatom-modified electrodes. Selecting electrolyte additives or solvents that are chemically inert toward heteroatoms can minimize side reactions and improve electrolyte stability. Furthermore, adjusting electrolyte properties, such as solvent polarity and salt concentration, can optimize ion transport kinetics and SEI formation on heteroatom-modified electrode surfaces. Furthermore, it is essential to consider the impact of heteroatoms on the interface between the electrode and the separator. Heteroatom-modified electrodes may exhibit altered wettability or adhesion properties, affecting ion transport across the electrode−separator interface and compromising battery performance. Engineering separator materials with tailored surface properties or modifying separator coatings can improve compatibility and ensure efficient ion transport, while maintaining electrode−separator stability. Therefore, ensuring the compatibility of HAIE with other battery components requires a profound understanding of the underlying mechanisms and meticulous optimization of the materials involved, including electrode, electrolyte, and separator materials.

Overall, it is crucial to address these challenges to realize the full potential of HAIE in advancing next-generation metal-based battery technologies. Continuous research and development are needed to overcome these obstacles and unlock the full benefits of heterogeneous atom immobilization engineering in metal-based batteries. Our findings and discussions highlight the importance of HAIE has been identified as a promising approach to advance the performance and durability of metal-based batteries, ultimately contributing to the development of more efficient and reliable energy storage solutions.

AUTHOR INFORMATION

Corresponding Authors

Yongzheng Zhang − *State Key Laboratory of Chemical Engineering, East China University of Science and Technology, 200237 Shanghai, China;* orcid.org/0000-0003-3889-1710; Email: zhangyongzheng@ecust.edu.cn

Zhiguo Du − *School of Materials Science and Engineering, Beihang University, 100191 Beijing, China;* orcid.org/0000-0001-9546-9458; Email: duzhiguo@buaa.edu.cn

Shubin Yang − *School of Materials Science and Engineering, Beihang University, 100191 Beijing, China;* orcid.org/0000-0001-9973-9785; Email: yangshubin@buaa.edu.cn

Meicheng Li − *State Key Laboratory of Alternate Electrical Power System with Renewable Energy Sources, School of New Energy, North China Electric Power University, 100096 Beijing, China;* orcid.org/0000-0002-0731-741X; Email: mcli@ncepu.edu.cn

Authors

Jianan Gu − *State Key Laboratory of Alternate Electrical Power System with Renewable Energy Sources, School of New Energy, North China Electric Power University, 100096 Beijing, China;* orcid.org/0000-0003-3914-5760

Yu Shi − *School of Materials Science and Engineering, Beihang University, 100191 Beijing, China*

Yilong Jin − *State Key Laboratory of Alternate Electrical Power System with Renewable Energy Sources, School of New Energy, North China Electric Power University, 100096 Beijing, China*

Hao Chen − *School of Materials Science and Engineering, Beihang University, 100191 Beijing, China*

Xin Sun − *State Key Laboratory of Alternate Electrical Power System with Renewable Energy Sources, School of New Energy, North China Electric Power University, 100096 Beijing, China*

Yanhong Wang − *State Key Laboratory of Alternate Electrical Power System with Renewable Energy Sources, School of New Energy, North China Electric Power University, 100096 Beijing, China*

Liang Zhan − *State Key Laboratory of Chemical Engineering, East China University of Science and Technology, 200237 Shanghai, China;* orcid.org/0000-0002-5640-7198

Complete contact information is available at: https://pubs.acs.org/10.1021/acsnano.4c08831

Notes

The authors declare no competing financial interest.

ACKNOWLEDGMENTS

This work is supported partially by project of National Natural Science Foundation of China (Grant nos. 52102203 and 51972110), Beijing Science and Technology Project (Z211100004621010), Beijing Natural Science Foundation (2222076), State Key Laboratory of Alternate Electrical Power System with Renewable Energy Sources (LAPS202114), Huaneng Group Headquarters Science and Technology Project (HNKJ20-H88), 2022 Strategic Research Key Project of Science and Technology Commission of the Ministry of Education, the Fundamental Research Funds for the Central Universities (No. 2024MS082), and the NCEPU "Double First-Class" Program.

VOCABULARY

Heteroatom immobilization engineering:A method for preparing single-atom supported materials by immobilizing heteroatoms

Nucleation and growth:Nucleation is the initial phase where atoms or molecules aggregate to form a stable nucleus, which then grows into a larger crystal.

https://doi.org/10.1021/acsnano.4c08831
ACS Nano 2024, 18, 25966−25985

Energy barrier:The energy threshold that must be overcome for atoms or molecules to migrate or for a reaction to proceed.
Desolvation:The process where solvated ions are reduced from a higher oxidation state to a zerovalent state, typically involving the removal of solvent molecules.
Side reaction:Unwanted reactions in electrochemical processes that can hinder the desired chemical reaction.

REFERENCES

(1) Wang, M.; Wang, B.; Zhang, J.; Xi, S.; Ling, N.; Mi, Z.; Yang, Q.; Zhang, M.; Leow, W. R.; Zhang, J.; et al. Acidic media enables oxygen-tolerant electrosynthesis of multicarbon products from simulated flue gas. *Nat. Commun.* **2024**, *15*, 1218.
(2) Wong, M.-K.; Foo, J. J.; Loh, J. Y.; Ong, W.-J. Leveraging Dual-Atom Catalysts for Electrocatalysis Revitalization: Exploring the Structure-Performance Correlation. *Adv. Energy Mater.* **2024**, *14*, No. 2303281.
(3) Xu, W.; Liu, H.-X.; Hu, Y.; Wang, Z.; Huang, Z.-Q.; Huang, C.; Lin, J.; Chang, C.-R.; Wang, A.; Wang, X.; et al. Metal-Oxo Electronic Tuning *via In Situ* CO Decoration for Promoting Methane Conversion to Oxygenates over Single-Atom Catalysts. *Angew. Chem., Int. Ed.* **2024**, *63*, No. e202315343.
(4) Zhang, H.; Zhang, S.; Guo, B.; Yu, L.-j.; Ma, L.; Hou, B.; Liu, H.; Zhang, S.; Wang, J.; Song, J.; et al. MoS_2 Hollow Multishelled Nanospheres Doped Fe Single Atoms Capable of Fast Phase Transformation for Fast-charging Na-ion Batteries. *Angew. Chem., Int. Ed.* **2024**, *63*, No. e202400285.
(5) Zhang, S.; Kong, Y.; Gu, Y.; Bai, R.; Li, M.; Zhao, S.; Ma, M.; Li, Z.; Zeng, L.; Qiu, D.; et al. Strong d-π Orbital Coupling of Co-C_4 Atomic Sites on Graphdiyne Boosts Potassium-Sulfur Battery Electrocatalysis. *J. Am. Chem. Soc.* **2024**, *146*, 4433−4443.
(6) Zhang, Y.-L.; Liu, B.; Dai, Y.-K.; Shen, L.-X.; Guo, P.; Xia, Y.-F.; Zhang, Z.; Kong, F.; Zhao, L.; Wang, Z.-B. Engineering Co-N-Cr Cross-Interfacial Electron Bridges to Break Activity-Stability Trade-Off for Superdurable Bifunctional Single Atom Oxygen Electrocatalysts. *Angew. Chem., Int. Ed.* **2024**, *63*, No. e202400577.
(7) Zhao, C.-X.; Liu, X.; Liu, J.-N.; Wang, J.; Wan, X.; Li, X.-Y.; Tang, C.; Wang, C.; Song, L.; Shui, J.; et al. Inductive Effect on Single-Atom Sites. *J. Am. Chem. Soc.* **2023**, *145*, 27531−27538.
(8) Zhao, X.; Zhang, Y.; Liu, W.; Zheng, Z.; Fu, Z.; Chen, C.; Hu, C. Understanding the Impact of Peripheral Substitution on the Activity of Co Phthalocyanine in Sulfur Reduction Catalysis. *Adv. Funct. Mater.* **2024**, *34*, No. 2313107.
(9) Zhong, J.; Liang, Z.; Liu, N.; Xiang, Y.; Yan, B.; Zhu, F.; Xie, X.; Gui, X.; Gan, L.; Yang, H. B.; et al. Engineering Symmetry-Breaking Centers and d-Orbital Modulation in Triatomic Catalysts for Zinc-Air Batteries. *ACS Nano* **2024**, *18*, 5258−5269.
(10) Zhou, E.; Luo, X.; Jin, H.; Wang, C.; Lu, Z.; Xie, Y.; Zhou, S.; Chen, Y.; He, Z.; Ma, R.; et al. Breaking Low-Strain and Deep-Potassiation Trade-Off in Alloy Anodes via Bonding Modulation for High-Performance K-Ion Batteries. *J. Am. Chem. Soc.* **2024**, *146*, 4752−4761.
(11) Zhu, S.; Ding, L.; Zhang, X.; Wang, K.; Wang, X.; Yang, F.; Han, G. Biaxially-Strained Phthalocyanine at Polyoxometalate@Carbon Nanotube Heterostructure Boosts Oxygen Reduction Catalysis. *Angew. Chem., Int. Ed.* **2023**, *62*, No. e202309545.
(12) Zong, L.; Fan, K.; Cui, L.; Lu, F.; Liu, P.; Li, B.; Feng, S.; Wang, L. Constructing Fe-N_4 Sites through Anion Exchange-mediated Transformation of Fe Coordination Environments in Hierarchical Carbon Support for Efficient Oxygen Reduction. *Angew. Chem., Int. Ed.* **2023**, *62*, No. e202309784.
(13) Feng, M.; Wu, X.; Cheng, H.; Fan, Z.; Li, X.; Cui, F.; Fan, S.; Dai, Y.; Lei, G.; He, G. Well-defined Fe-Cu diatomic sites for efficient catalysis of CO_2 electroreduction. *J. Mater. Chem. A* **2021**, *9*, 23817.
(14) Zhang, Z.; Xu, X. Efficient Heteronuclear Diatom Electrocatalyst for Nitrogen Reduction Reaction: Pd-Nb Diatom Supported on Black Phosphorus. *ACS Appl. Mater. Interfaces* **2020**, *12*, 56987−56994.
(15) Zhu, C.; Cun, F.; Fan, Z.; Nie, Y.; Du, Q.; Liu, F.; Yang, W.; Li, A. Heterogeneous Fe-Co dual-atom catalyst outdistances the homogeneous counterpart for peroxymonosulfate-assisted water decontamination: New surface collision oxidation path and diatomic synergy. *Water Res.* **2023**, *241*, No. 120164.
(16) Li, Z.; Li, B.; Li, Q. Single-Atom Nano-Islands (SANIs): A Robust Atomic-Nano System for Versatile Heterogeneous Catalysis Applications. *Adv. Mater.* **2023**, *35*, No. 2211103.
(17) Huang, J.-R.; Shi, W.-X.; Xu, S.-Y.; Luo, H.; Zhang, J.; Lu, T.-B.; Zhang, Z.-M. Water-Mediated Selectivity Control of CH_3OH versus CO/CH_4 in CO_2 Photoreduction on Single-Atom Implanted Nanotube Arrays. *Adv. Mater.* **2024**, *36*, No. 2306906.
(18) Liu, L.; Hu, J.; Ma, Z.; Zhu, Z.; He, B.; Chen, F.; Lu, Y.; Xu, R.; Zhang, Y.; Ma, T.; et al. One-dimensional single atom arrays on ferroelectric nanosheets for enhanced CO_2 photoreduction. *Nat. Commun.* **2024**, *15*, 305.
(19) Ma, Z.; Zhang, T.; Lin, L.; Han, A.; Liu, J. Ni single-atom arrays as self-supported electrocatalysts for CO_2RR. *AIChE J.* **2023**, *69*, No. e18161.
(20) Liu, K.; Li, H.; Xie, M.; Wang, P.; Jin, Z.; Liu, Y.; Zhou, M.; Li, P.; Yu, G. Thermally Enhanced Relay Electrocatalysis of Nitrate-to-Ammonia Reduction over Single-Atom-Alloy Oxides. *J. Am. Chem. Soc.* **2024**, *146*, 7779−7790.
(21) Shirani, J.; Valdes, J. J.; Tchagang, A. B.; Bevan, K. H. Adsorbate-Dependent Electronic Structure Descriptors for Machine Learning-Driven Binding Energy Predictions in Diverse Single Atom Alloys: A Reductionist Approach. *J. Phys. Chem. C* **2024**, *128*, 4483.
(22) Xiang, J.; Qiang, C.; Shang, S.; Chen, K.; Kang, C.; Chu, K. Tandem Electrocatalytic Reduction of Nitrite to Ammonia on Rhodium-Copper Single Atom Alloys. *Adv. Funct. Mater.* **2024**, No. 2401941.
(23) Yin, J.-Q.; Nakajima, T.; Sakaki, S. Catalysis of Nickel-Based gold single-atom alloy for NO-CO reaction: Theoretical insight into role of gold atom in enhancing catalytic activity. *J. Catal.* **2024**, *432*, No. 115430.
(24) De, S.; Mondal, A.; Giblin, S. R.; Layfield, R. A. Bimetallic Synergy Enables Silole Insertion into THF and the Synthesis of Erbium Single-Molecule Magnets. *Angew. Chem., Int. Ed.* **2024**, *63*, No. e202317678.
(25) Fang, Y.; Wei, C.; Bian, Z.; Yin, X.; Liu, B.; Liu, Z.; Chi, P.; Xiao, J.; Song, W.; Niu, S.; et al. Unveiling the nature of Pt-induced anti-deactivation of Ru for alkaline hydrogen oxidation reaction. *Nat. Commun.* **2024**, *15*, 1614.
(26) Hojo, H.; Nakashima, M.; Yoshizaki, S.; Einaga, H. Lattice-Plane-Dependent Distribution of Ce^{3+} at Pt and CeO_2 Interfaces for Pt/CeO_2 Catalysts. *ACS Nano* **2024**, *18*, 4775−4782.
(27) Lin, X.; Zhang, X.; Liu, D.; Shi, L.; Zhao, L.; Long, Y.; Dai, L. Asymmetric Atomic Tin Catalysts with Tailored p-Orbital Electron Structure for Ultra-Efficient Oxygen Reduction. *Adv. Energy Mater.* **2024**, *14*, No. 2303740.
(28) Song, W.; Yang, X.; Zhang, T.; Huang, Z.; Wang, H.; Sun, J.; Xu, Y.; Ding, J.; Hu, W. Optimizing potassium polysulfides for high performance potassium-sulfur batteries. *Nat. Commun.* **2024**, *15*, 1005.
(29) Balamurugan, J.; Austeria, P. M.; Kim, J. B.; Jeong, E.-S.; Huang, H.-H.; Kim, D. H.; Koratkar, N.; Kim, S. O. Electrocatalysts for Zinc-Air Batteries Featuring Single Molybdenum Atoms in a Nitrogen-Doped Carbon Framework. *Adv. Mater.* **2023**, *35*, No. 2302625.
(30) Baumert, M. E.; Le, V.; Su, P.-H.; Akae, Y.; Bresser, D.; Theato, P.; Hansmann, M. M. From Squaric Acid Amides (SQAs) to Quinoxaline-Based SQAs——Evolution of a Redox-Active Cathode Material for Organic Polymer Batteries. *J. Am. Chem. Soc.* **2023**, *145*, 23334−23345.
(31) Cai, J.; Zhang, H.; Zhang, L.; Xiong, Y.; Ouyang, T.; Liu, Z.-Q. Hetero-Anionic Structure Activated Co-S Bonds Promote Oxygen

https://doi.org/10.1021/acsnano.4c08831
ACS Nano 2024, 18, 25966−25985

Electrocatalytic Activity for High-Efficiency Zinc-Air Batteries. *Adv. Mater.* **2023**, *35*, No. 2303488.
(32) Cui, K.; Tang, X.; Xu, X.; Kou, M.; Lyu, P.; Xu, Y. Crystalline Dual-Porous Covalent Triazine Frameworks as a New Platform for Efficient Electrocatalysis. *Angew. Chem., Int. Ed.* **2024**, *63*, No. e202317664.
(33) Deng, Q.; Yang, Y.; Yin, K.; Yi, J.; Zhou, Y.; Zhang, Y. Boosting Active Species Ru-O-Zr/Ce Construction at the Interface of Phase-Transformed Zirconia-Ceria Isomerism toward Advanced Catalytic Cathodes for Li-CO_2 Batteries. *Adv. Energy Mater.* **2023**, *13*, No. 2302398.
(34) Zhao, Y.; Feng, K.; Yu, Y. A review on covalent organic frameworks as artificial interface layers for Li and Zn metal anodes in rechargeable batteries. *Adv. Sci.* **2024**, *11*, No. 2308087.
(35) Zhao, Y.; Yang, C.; Yu, Y. A review on covalent organic frameworks for rechargeable zinc-ion batteries. *Chin. Chem. Lett.* **2024**, *35*, No. 108865.
(36) Dey, G.; Jana, R.; Saifi, S.; Kumar, R.; Bhattacharyya, D.; Datta, A.; Sinha, A. S. K.; Aijaz, A. Dual Single-Atomic Co-Mn Sites in Metal-Organic-Framework-Derived N-Doped Nanoporous Carbon for Electrochemical Oxygen Reduction. *ACS Nano* **2023**, *17*, 19155−19167.
(37) Fan, W.; Li, P.; Shi, J.; Chen, J.; Tian, W.; Wang, H.; Wu, J.; Yu, G. Atomic Zincophilic Sites Regulating Microspace Electric Fields for Dendrite-Free Zinc Anode. *Adv. Mater.* **2024**, *36*, No. 2307219.
(38) Feng, L.; Yan, R.; Sun, X.-R.; Zhu, Z.; Jia, W.; Yan, X.; Yang, Y.-Y.; Li, S.; Fu, X.; Yang, W.; et al. Cell-Membrane Inspired Multifunctional Nanocoating for Rescuing the Active-Material Microenvironment in High-Capacity Sulfur Cathode. *Adv. Energy Mater.* **2024**, *14*, No. 2303848.
(39) Guo, N.; Xue, H.; Ren, R.; Sun, J.; Song, T.; Dong, H.; Zhao, Z.; Zhang, J.; Wang, Q.; Wu, L. S-Block Potassium Single-atom Electrocatalyst with K-N_4 Configuration Derived from K^+/Polydopamine for Efficient Oxygen Reduction. *Angew. Chem., Int. Ed.* **2023**, *62*, No. e202312409.
(40) Guo, X.; Shi, J.; Li, M.; Zhang, J.; Zheng, X.; Liu, Y.; Xi, B.; An, X.; Duan, Z.; Fan, Q.; et al. Modulating Coordination of Iron Atom Clusters on N,P,S Triply-Doped Hollow Carbon Support towards Enhanced Electrocatalytic Oxygen Reduction. *Angew. Chem., Int. Ed.* **2023**, *62*, No. e202314124.
(41) He, Q.; Li, Z.; Wu, M.; Xie, M.; Bu, F.; Zhang, H.; Yu, R.; Mai, L.; Zhao, Y. Ultra-Uniform and Functionalized Nano-Ion Divider for Regulating Ion Distribution toward Dendrite-Free Lithium-Metal Batteries. *Adv. Mater.* **2023**, *35*, No. 2302418.
(42) Jiao, S.; Sun, Y.; Wang, J.; Shi, D.; Li, Y.; Jiang, X.; Wang, F.; Zhang, Y.; Liu, J.; Wang, X.; et al. The Mechanism of Fluorine Doping for the Enhanced Lithium Storage Behavior in Cation-Disordered Cathode Oxide. *Adv. Energy Mater.* **2023**, *13*, No. 2301636.
(43) Jing, Q.; Mei, Z.; Sheng, X.; Zou, X.; Xu, Q.; Wang, L.; Guo, H. Tuning the Bonding Behavior of d-p Orbitals to Enhance Oxygen Reduction through Push-Pull Electronic Effects. *Adv. Funct. Mater.* **2024**, *34*, No. 2307002.
(44) Lee, D. G.; Cho, J. Y.; Kim, J. H.; Ryoo, G.; Yoon, J.; Jo, A.; Lee, M. H.; Park, J. H.; Yoo, J.-K.; Lee, D. Y.; et al. Dispersant-Free Colloidal and Interfacial Engineering of Si-Nanocarbon Hybrid Anode Materials for High-Performance Li-Ion Batteries. *Adv. Funct. Mater.* **2024**, *34*, No. 2311353.
(45) Lee, K.; Kim, E. J.; Kim, J.; Kim, K. H.; Lee, Y. J.; Lee, M. J.; Ryu, K.; Shin, S.; Choi, J.; Kwon, S. H.; et al. Coordination Engineering of N, O Co-Doped Cu Single Atom on Porous Carbon for High Performance Zinc Metal Anodes. *Adv. Energy Mater.* **2024**, *14*, No. 2303803.
(46) Li, H.; Wang, W.; Xue, S.; He, J.; Liu, C.; Gao, G.; Di, S.; Wang, S.; Wang, J.; Yu, Z.; et al. Superstructure-Assisted Single-Atom Catalysis on Tungsten Carbides for Bifunctional Oxygen Reactions. *J. Am. Chem. Soc.* **2024**, *146*, 9124−9133.
(47) Li, R.; Fan, W.; Rao, P.; Luo, J.; Li, J.; Deng, P.; Wu, D.; Huang, W.; Jia, C.; Liu, Z.; et al. Multimetallic Single-Atom Catalysts for Bifunctional Oxygen Electrocatalysis. *ACS Nano* **2023**, *17*, 18128−18138.
(48) Liang, C.; Han, X.; Zhang, T.; Dong, B.; Li, Y.; Zhuang, Z.; Han, A.; Liu, J. Cu Nanoclusters Accelerate the Rate-Determining Step of Oxygen Reduction on Fe——N——C in All pH Range. *Adv. Energy Mater.* **2024**, *14*, No. 2303935.
(49) Liang, Q.; Wang, S.; Lu, X.; Jia, X.; Yang, J.; Liang, F.; Xie, Q.; Yang, C.; Qian, J.; Song, H.; et al. High-Entropy MXene as Bifunctional Mediator toward Advanced Li-S Full Batteries. *ACS Nano* **2024**, *18*, 2395−2408.
(50) Liu, M.; Zhang, J.; Su, H.; Jiang, Y.; Zhou, W.; Yang, C.; Bo, S.; Pan, J.; Liu, Q. In situ modulating coordination fields of single-atom cobalt catalyst for enhanced oxygen reduction reaction. *Nat. Commun.* **2024**, *15*, 1675.
(51) Lyu, L.; Hu, X.; Lee, S.; Fan, W.; Kim, G.; Zhang, J.; Zhou, Z.; Kang, Y.-M. Oxygen Reduction Kinetics of Fe-N-C Single Atom Catalysts Boosted by Pyridinic N Vacancy for Temperature-Adaptive Zn-Air Batteries. *J. Am. Chem. Soc.* **2024**, *146*, 4803−4813.
(52) Pei, Z.; Zhang, H.; Guo, Y.; Luan, D.; Gu, X.; Lou, X. W. Atomically Dispersed Fe Sites Regulated by Adjacent Single Co Atoms Anchored on N-P Co-Doped Carbon Structures for Highly Efficient Oxygen Reduction Reaction. *Adv. Mater.* **2024**, *36*, No. 2306047.
(53) Qi, C.; Yang, H.; Sun, Z.; Wang, H.; Xu, N.; Zhu, G.; Wang, L.; Jiang, W.; Yu, X.; Li, X.; et al. Modulating Electronic Structures of Iron Clusters through Orbital Rehybridization by Adjacent Single Copper Sites for Efficient Oxygen Reduction. *Angew. Chem., Int. Ed.* **2023**, *62*, No. e202308344.
(54) Ran, L.; Xu, Y.; Zhu, X.; Chen, S.; Qiu, X. Mn Single-Atom Tuning Fe-N-C Catalyst Enables Highly Efficient and Durable Oxygen Electrocatalysis and Zinc-Air Batteries. *ACS Nano* **2024**, *18*, 750−760.
(55) Song, L.-N.; Zheng, L.-J.; Wang, X.-X.; Kong, D.-C.; Wang, Y.-F.; Wang, Y.; Wu, J.-Y.; Sun, Y.; Xu, J.-J. Aprotic Lithium-Oxygen Batteries Based on Nonsolid Discharge Products. *J. Am. Chem. Soc.* **2024**, *146*, 1305−1317.
(56) Sun, T.; Huang, F.; Liu, J.; Yu, H.; Feng, X.; Feng, X.; Yang, Y.; Shu, H.; Zhang, F. Strengthened d-p Orbital-Hybridization of Single Atoms with Sulfur Species Induced Bidirectional Catalysis for Lithium-Sulfur Batteries. *Adv. Funct. Mater.* **2023**, *33*, No. 2306049.
(57) Sun, Y.; Wang, J.; Shang, T.; Li, Z.; Li, K.; Wang, X.; Luo, H.; Lv, W.; Jiang, L.; Wan, Y. Counting *d*-Orbital Vacancies of Transition-Metal Catalysts for the Sulfur Reduction Reaction. *Angew. Chem., Int. Ed.* **2023**, *62*, No. e202306791.
(58) Tang, D.; Ji, G.; Wang, J.; Liang, Z.; Chen, W.; Ji, H.; Ma, J.; Liu, S.; Zhuang, Z.; Zhou, G. A Multifunctional Amino Acid Enables Direct Recycling of Spent $LiFePO_4$ Cathode Material. *Adv. Mater.* **2024**, *36*, No. 2309722.
(59) Wang, J.; Zhang, J.; Wu, J.; Huang, M.; Jia, L.; Li, L.; Zhang, Y.; Hu, H.; Liu, F.; Guan, Q.; et al. Interfacial "Single-Atom-in-Defects" Catalysts Accelerating Li^+ Desolvation Kinetics for Long-Lifespan Lithium-Metal Batteries. *Adv. Mater.* **2023**, *35*, No. 2302828.
(60) Wang, R.; Qin, J.; Pei, F.; Li, Z.; Xiao, P.; Huang, Y.; Yuan, L.; Wang, D. Ni Single Atoms on Hollow Nanosheet Assembled Carbon Flowers Optimizing Polysulfides Conversion for Li-S Batteries. *Adv. Funct. Mater.* **2023**, *33*, No. 2305991.
(61) Wen, X.; Feng, W.; Li, X.; Yang, J.; Du, R.; Wang, P.; Li, H.; Song, L.; Wang, Y.; Cheng, M.; et al. Diatomite-Templated Synthesis of Single-Atom Cobalt-Doped MoS_2/Carbon Composites to Boost Sodium Storage. *Adv. Mater.* **2023**, *35*, No. 2211690.
(62) Xu, W.; Li, H.; Zhang, X.; Chen, T.-Y.; Yang, H.; Min, H.; Shen, X.; Chen, H.-Y.; Wang, J. Regulating Graphitic Microcrystalline and Single-Atom Chemistry in Hard Carbon Enables High-Performance Potassium Storage. *Adv. Funct. Mater.* **2024**, *34*, No. 2309509.
(63) Zhang, C.; Xie, J.; Zhao, C.; Yang, Y.; An, Q.; Mei, Z.; Xu, Q.; Ding, Y.; Zhao, G.; Guo, H. Regulating the Lithium Ions' Local Coordination Environment through Designing a COF with Single Atomic Co Site to Achieve Dendrite-Free Lithium-Metal Batteries. *Adv. Mater.* **2023**, *35*, No. 2304511.

https://doi.org/10.1021/acsnano.4c08831
ACS Nano 2024, 18, 25966−25985

(64) Balaish, M.; Gonzalez-Rosillo, J. C.; Kim, K. J.; Zhu, Y.; Hood, Z. D.; Rupp, J. L. M. Processing thin but robust electrolytes for solid-state batteries. *Nat. Energy* **2021**, *6*, 227−239.
(65) Janek, J.; Zeier, W. G. Challenges in speeding up solid-state battery development. *Nat. Energy* **2023**, *8*, 230−240.
(66) Xiao, J.; Shi, F.; Glossmann, T.; Burnett, C.; Liu, Z. From laboratory innovations to materials manufacturing for lithium-based batteries. *Nat. Energy* **2023**, *8*, 329−339.
(67) Cai, Z.; Ouyang, B.; Hau, H.-M.; Chen, T.; Giovine, R.; Koirala, K. P.; Li, L.; Ji, H.; Ha, Y.; Sun, Y.; et al. In situ formed partially disordered phases as earth-abundant Mn-rich cathode materials. *Nat. Energy* **2024**, *9*, 27−36.
(68) Huang, Z.; Lai, J.-C.; Liao, S.-L.; Yu, Z.; Chen, Y.; Yu, W.; Gong, H.; Gao, X.; Yang, Y.; Qin, J.; et al. A salt-philic, solvent-phobic interfacial coating design for lithium metal electrodes. *Nat. Energy* **2023**, *8*, 577−585.
(69) Lei, J.; Zhang, Y.; Yao, Y.; Shi, Y.; Leung, K. L.; Fan, J.; Lu, Y.-C. An active and durable molecular catalyst for aqueous polysulfide-based redox flow batteries. *Nat. Energy* **2023**, *8*, 1355−1364.
(70) Duan, H.; You, Y.; Wang, G.; Ou, X.; Wen, J.; Huang, Q.; Lyu, P.; Liang, Y.; Li, Q.; Huang, J.; et al. Lithium-Ion Charged Polymer Channels Flattening Lithium Metal Anode. *Nano-micro Lett.* **2024**, *16*, 78.
(71) Yan, H.; Li, S.; Zhong, J.; Li, B. An Electrochemical Perspective of Aqueous Zinc Metal Anode. *Nano-micro Lett.* **2024**, *16*, 15.
(72) Huang, Z.; Yang, S.; Zhang, Y.; Zhang, Y.; Xue, R.; Ma, Y.; Wang, Z. Ultrathin Reed Membranes: Nature's Intimate Ion-Regulation Skins Safeguarding Zinc Metal Anodes in Aqueous Batteries. *Adv. Energy Mater.* **2024**, *14*, No. 2400033.
(73) Kim, K.; Ko, Y.; Tamwattana, O.; Kim, Y.; Kim, J.; Park, J.; Han, S.; Lee, Y.-R.; Kang, K. Macroscale Inhomogeneity in Electrochemical Lithium-Metal Plating Triggered by Electrolyte-Dependent Gas Phase Evolution. *Adv. Energy Mater.* **2024**, *14*, No. 2304396.
(74) Qiao, H.; Zhu, X.; Li, X.; Wang, Y.; Ye, C.; Ma, L.; Shen, J.; Ye, M. Uncovering Synergistic Effects of Electrode/Electrolyte Toward Concerted Cathodic Structure Stabilization for Superior-Performance Aqueous Zn-δ-MnO_2 Battery. *Adv. Energy Mater.* **2024**, *14*, No. 2304357.
(75) Gu, J.; Tao, Y.; Chen, H.; Cao, Z.; Zhang, Y.; Du, Z.; Cui, Y.; Yang, S. Stress-Release Functional Liquid Metal-MXene Layers toward Dendrite-Free Zinc Metal Anodes. *Adv. Energy Mater.* **2022**, *12*, No. 2200115.
(76) Gu, J.; Zhu, Q.; Shi, Y.; Chen, H.; Zhang, D.; Du, Z.; Yang, S. Single Zinc Atoms Immobilized on MXene ($Ti_3C_2Cl_x$) Layers toward Dendrite-Free Lithium Metal Anodes. *ACS Nano* **2020**, *14*, 891−898.
(77) Shi, Y.; Li, B.; Zhang, Y.; Cui, Y.; Cao, Z.; Du, Z.; Gu, J.; Shen, K.; Yang, S. Tortuosity Modulation toward High-Energy and High-Power Lithium Metal Batteries. *Adv. Energy Mater.* **2021**, *11*, No. 2003663.
(78) Zhu, X.; Cheng, H.; Lyu, S.; Huang, J.; Gu, J.; Guo, Y.; Peng, Y.; Liu, J.; Wang, C.; Duan, J.; et al. High-Energy-Heavy-Ion Engineering Low-Tortuosity and High-Porosity 3D Metallic Electrodes for Long-Life Lithium Anodes. *Adv. Energy Mater.* **2023**, *13*, No. 2300129.
(79) Xu, K.; Zhu, M.; Wu, X.; Liang, J.; Liu, Y.; Zhang, T.; Zhu, Y.; Qian, Y. Dendrite-tamed deposition kinetics using single-atom Zn sites for Li metal anode. *Energy Storage Mater.* **2019**, *23*, 587−593.
(80) Yang, T.; Qian, T.; Sun, Y.; Zhong, J.; Rosei, F.; Yan, C. Mega high utilization of sodium metal anodes enabled by single zinc atom sites. *Nano Lett.* **2019**, *19*, 7827−7835.
(81) Gu, J.; Zhu, Q.; Shi, Y.; Chen, H.; Zhang, D.; Du, Z.; Yang, S. Single Zinc Atoms Immobilized on MXene ($Ti_3C_2Cl_x$) Layers toward Dendrite-Free Lithium Metal Anodes. *ACS Nano* **2020**, *14*, 891−898.
(82) Song, C.-L.; Li, Z.-H.; Ma, L.-Y.; Li, M.-Z.; Huang, S.; Hong, X.-J.; Cai, Y.-P.; Lan, Y.-Q. Single-atom zinc and anionic framework as janus separator coatings for efficient inhibition of lithium dendrites and shuttle effect. *ACS Nano* **2021**, *15*, 13436−13443.
(83) Chen, S.; Chen, J.; Liao, X.; Li, Y.; Wang, W.; Huang, R.; Zhao, T.; Yan, S.; Yan, Z.; Cheng, F. Enabling low-temperature and high-rate Zn metal batteries by activating Zn nucleation with single-atomic sites. *ACS Energy Lett.* **2022**, *7*, 4028−4035.
(84) Bai, R.; Lin, Q.; Li, X.; Ling, F.; Wang, H.; Tan, S.; Hu, L.; Ma, M.; Wu, X.; Shao, Y. Toward Complete Transformation of Sodium Polysulfides by Regulating the Second-Shell Coordinating Environment of Atomically Dispersed Fe. *Angew. Chem., Int. Ed.* **2023**, *135*, No. e202218165.
(85) Lee, K.; Kim, E. J.; Kim, J.; Kim, K. H.; Lee, Y. J.; Lee, M. J.; Ryu, K.; Shin, S.; Choi, J.; Kwon, S. H. Coordination Engineering of N, O Co-Doped Cu Single Atom on Porous Carbon for High Performance Zinc Metal Anodes. *Adv. Energy Mater.* **2024**, *14*, No. 2303803.
(86) Yang, Z.; Dang, Y.; Zhai, P.; Wei, Y.; Chen, Q.; Zuo, J.; Gu, X.; Yao, Y.; Wang, X.; Zhao, F. Single-atom reversible lithiophilic sites toward stable lithium anodes. *Adv. Energy Mater.* **2022**, *12*, No. 2103368.
(87) Li, Y.; Fang, D.; Li, X. L.; Yan, D.; Xi, S.; Li, T. C.; Lin, C.; Huang, S.; Qiu, J.; Xu, X. Asymmetric N, O-Coordinated Single Atomic Co Sites for Stable Lithium Metal Anodes. *Energy Environ. Mater.* **2023**, *6*, No. e12449.
(88) Yang, Z.; Lai, F.; Mao, Q.; Liu, C.; Wang, R.; Lu, Z.; Zhang, T.; Liu, X. Reversing Zincophobic/Hydrophilic Nature of Metal-N-C via Metal-Coordination Interaction for Dendrite-Free Zn Anode with High Depth-of-Discharge. *Adv. Mater.* **2024**, *36*, No. 2311637.
(89) Zhang, C.; Xie, J.; Zhao, C.; Yang, Y.; An, Q.; Mei, Z.; Xu, Q.; Ding, Y.; Zhao, G.; Guo, H. Regulating the Lithium Ions' Local Coordination Environment through Designing a COF with Single Atomic Co Site to Achieve Dendrite-Free Lithium-Metal Batteries. *Adv. Mater.* **2023**, *35*, No. 2304511.
(90) Li, X.; Ye, W.; Xu, P.; Huang, H.; Fan, J.; Yuan, R.; Zheng, M. S.; Wang, M. S.; Dong, Q. An Encapsulation-Based Sodium Storage via Zn-Single-Atom Implanted Carbon Nanotubes. *Adv. Mater.* **2022**, *34*, No. 2202898.
(91) Liu, H.; Chen, X.; Cheng, X.-B.; Li, B.-Q.; Zhang, R.; Wang, B.; Chen, X.; Zhang, Q. Uniform Lithium Nucleation Guided by Atomically Dispersed Lithiophilic CoNx Sites for Safe Lithium Metal Batteries. *Small Methods* **2019**, *3*, No. 1800354.
(92) Liang, Z.; Peng, C.; Shen, J.; Yang, Y.; Yao, S.; Xue, D.; Zhu, M.; Liu, J. Lithiophilic single-atom Co on carbon nanosheets synergistically modulates Li deposition enable dendrite-free lithium metal batteries. *J. Power Sources* **2023**, *556*, No. 232474.
(93) Yan, K.; Lu, Z.; Lee, H.-W.; Xiong, F.; Hsu, P.-C.; Li, Y.; Zhao, J.; Chu, S.; Cui, Y. Selective deposition and stable encapsulation of lithium through heterogeneous seeded growth. *Nat. Energy* **2016**, *1*, 1−8.
(94) Tao, Y.; Zuo, S. W.; Xiao, S. H.; Sun, P. X.; Li, N. W.; Chen, J. S.; Zhang, H. B.; Yu, L. Atomically dispersed Cu in zeolitic imidazolate framework nanoflake array for dendrite-free Zn metal anode. *Small* **2022**, *18*, No. 2203231.
(95) Zhang, D.; Ma, X.; Wu, L.; Wen, J.; Li, F.; Zhou, J.; Rao, A. M.; Lu, B. Coupling Low-Tortuosity Carbon Matrix with Single-Atom Chemistry Enables Dendrite-Free Potassium-Metal Anode. *Adv. Energy Mater.* **2023**, *13*, No. 2203277.
(96) Cui, J.; Jin, B.; Xu, A.; Li, J.; Shao, M. Single-Atom Metallophilic Sites for Liquid NaK Alloy Confinement toward Stable Alkali-Metal Anodes. *Adv. Sci.* **2023**, *10*, No. 2206479.
(97) Shi, H.; Li, Y.; Lu, P.; Wu, Z.-S. Single-atom cobalt coordinated to oxygen sites on graphene for stable lithium metal anodes. *Acta Phys.-Chim. Sin.* **2020**, *0*, 2008033−2008030.
(98) Huang, W.; Liu, S.; Yu, R.; Zhou, L.; Liu, Z.; Mai, L. Single-Atom Lithiophilic Sites Confined within Ordered Porous Carbon for Ultrastable Lithium Metal Anodes. *Energy Environ. Mater.* **2023**, *6*, No. e12466.
(99) Sun, Y.; Zhou, J.; Ji, H.; Liu, J.; Qian, T.; Yan, C. Single-Atom Iron as Lithiophilic Site To Minimize Lithium Nucleation Overpotential for Stable Lithium Metal Full Battery. *ACS Appl. Mater. Interfaces* **2019**, *11*, 32008−32014.

https://doi.org/10.1021/acsnano.4c08831
ACS Nano 2024, 18, 25966−25985

(100) Zhou, L.; Yang, F.; Zeng, S.; Gao, X.; Liu, X.; Cao, X.; Yu, P.; Lu, X. Zincophilic Cu sites induce dendrite-free Zn anodes for robust alkaline/neutral aqueous batteries. *Adv. Funct. Mater.* **2022**, *32*, No. 2110829.
(101) Fan, W.; Li, P.; Shi, J.; Chen, J.; Tian, W.; Wang, H.; Wu, J.; Yu, G. Atomic Zincophilic Sites Regulating Microspace Electric Fields for Dendrite-Free Zinc Anode. *Adv. Mater.* **2024**, *36*, No. 2307219.
(102) Li, Y.; Lin, S.; Wang, D.; Gao, T.; Song, J.; Zhou, P.; Xu, Z.; Yang, Z.; Xiao, N.; Guo, S. Single atom array mimic on ultrathin MOF nanosheets boosts the safety and life of lithium-sulfur batteries. *Adv. Mater.* **2020**, *32*, No. 1906722.
(103) Huang, T.; Sun, Y.; Wu, J.; Jin, J.; Wei, C.; Shi, Z.; Wang, M.; Cai, J.; An, X.-T.; Wang, P. A Dual-Functional Fibrous Skeleton Implanted with Single-Atomic Co−N_x Dispersions for Longevous Li−S Full Batteries. *ACS Nano* **2021**, *15*, 14105−14115.
(104) Wang, J.; Zhang, J.; Cheng, S.; Yang, J.; Xi, Y.; Hou, X.; Xiao, Q.; Lin, H. Long-life dendrite-free lithium metal electrode achieved by constructing a single metal atom anchored in a diffusion modulator layer. *Nano Lett.* **2021**, *21*, 3245−3253.
(105) Song, P.; Zheng, S.; Ullah, Z.; Yang, Z.; Zhu, P.; He, A.; Wang, C.; Li, Q. Synergistic Effects of FeCo Bimetallic Single-Atom Catalysts: Accelerating the Redox Conversion of Polysulfides and Inhibiting the Growth of Lithium Dendrites in Lithium−Sulfur Batteries. *ACS Appl. Energy Mater.* **2023**, *6*, 4671−4682.
(106) Shi, H.; Ren, X.; Lu, J.; Dong, C.; Liu, J.; Yang, Q.; Chen, J.; Wu, Z. S. Dual-functional atomic zinc decorated hollow carbon nanoreactors for kinetically accelerated polysulfides conversion and dendrite free lithium sulfur batteries. *Adv. Energy Mater.* **2020**, *10*, No. 2002271.
(107) Yuan, J.; Xi, B.; Wang, P.; Zhang, Z.; Song, N.; An, X.; Liu, J.; Feng, J.; Xiong, S. Multifunctional Atomic Molybdenum on Graphene with Distinctive Coordination to Solve Li and S Electrochemistry. *Small* **2022**, *18*, No. 2203947.
(108) Li, Y.; Gao, T.; Ni, D.; Zhou, Y.; Yousaf, M.; Guo, Z.; Zhou, J.; Zhou, P.; Wang, Q.; Guo, S. Two birds with one stone: Interfacial engineering of multifunctional janus separator for lithium−sulfur batteries. *Adv. Mater.* **2022**, *34*, No. 2107638.
(109) Zhang, E.; Hu, X.; Meng, L.; Qiu, M.; Chen, J.; Liu, Y.; Liu, G.; Zhuang, Z.; Zheng, X.; Zheng, L. Single-Atom Yttrium Engineering Janus Electrode for Rechargeable Na−S Batteries. *J. Am. Chem. Soc.* **2022**, *144*, 18995−19007.
(110) Hu, P.; Xiao, F.; Wang, H.; Rogach, A. L. Dual-functional hosts derived from metal-organic frameworks reduce dissolution of polyselenides and inhibit dendrite growth in a sodium-selenium battery. *Energy Storage Mater.* **2022**, *51*, 249−258.
(111) Zhang, J.; Wang, E.; Cui, S.; Yang, S.; Zou, X.; Gong, Y. Single-Atom Pt Anchored on Oxygen Vacancy of Monolayer Ti3C2T x for Superior Hydrogen Evolution. *Nano Lett.* **2022**, *22*, 1398−1405.
(112) Zhang, J.; Zhao, Y.; Guo, X.; Chen, C.; Dong, C.-L.; Liu, R.-S.; Han, C.-P.; Li, Y.; Gogotsi, Y.; Wang, G. Single platinum atoms immobilized on an MXene as an efficient catalyst for the hydrogen evolution reaction. *Nat. Catal.* **2018**, *1*, 985−992.
(113) Zhao, D.; Chen, Z.; Yang, W.; Liu, S.; Zhang, X.; Yu, Y.; Cheong, W.-C.; Zheng, L.; Ren, F.; Ying, G. MXene (Ti_3C_2) vacancy-confined single-atom catalyst for efficient functionalization of CO_2. *J. Am. Chem. Soc.* **2019**, *141*, 4086−4093.
(114) Zhao, Q.; Zhang, C.; Hu, R.; Du, Z.; Gu, J.; Cui, Y.; Chen, X.; Xu, W.; Cheng, Z.; Li, S.; et al. Selective Etching Quaternary MAX Phase toward Single Atom Copper Immobilized MXene ($Ti_3C_2Cl_x$) for Efficient CO_2 Electroreduction to Methanol. *ACS Nano* **2021**, *15*, 4927−4936.
(115) Zhang, D.; Wang, S.; Hu, R.; Gu, J.; Cui, Y.; Li, B.; Chen, W.; Liu, C.; Shang, J.; Yang, S. Catalytic conversion of polysulfides on single atom zinc implanted MXene toward high-rate lithium−sulfur batteries. *Adv. Funct. Mater.* **2020**, *30*, No. 2002471.
(116) Song, H.; Du, R.; Wang, Y.; Zu, D.; Zhou, R.; Cai, Y.; Wang, F.; Li, Z.; Shen, Y.; Li, C. Anchoring single atom cobalt on two-dimensional MXene for activation of peroxymonosulfate. *Appl. Catal. B Environ.* **2021**, *286*, No. 119898.
(117) Chen, W.; Li, P.; Yu, J.; Cui, P.; Yu, X.; Song, W.; Cao, C. In-situ doping nickel single atoms in two-dimensional MXenes analogue support for room temperature NO_2 sensing. *Nano Res.* **2022**, *15*, 9544−9553.
(118) Yang, P.; Long, Y.; Huang, W.; Liu, D. Single-atom copper embedded in two-dimensional MXene toward peroxymonosulfate activation to generate singlet oxygen with nearly 100% selectivity for enhanced Fenton-like reactions. *Appl. Catal. B Environ.* **2023**, *324*, No. 122245.
(119) Zhang, D.; Wang, S.; Hu, R.; Gu, J.; Cui, Y.; Li, B.; Chen, W.; Liu, C.; Shang, J.; Yang, S. Catalytic Conversion of Polysulfides on Single Atom Zinc Implanted MXene toward High-Rate Lithium-Sulfur Batteries. *Adv. Funct. Mater.* **2020**, *30*, No. 2002471.
(120) Li, M.; Lu, J.; Luo, K.; Li, Y.; Chang, K.; Chen, K.; Zhou, J.; Rosen, J.; Hultman, L.; Eklund, P.; et al. Element Replacement Approach by Reaction with Lewis Acidic Molten Salts to Synthesize Nanolaminated MAX Phases and MXenes. *J. Am. Chem. Soc.* **2019**, *141*, 4730−4737.

https://doi.org/10.1021/acsnano.4c08831
ACS Nano 2024, 18, 25966−25985